15 August 2024
lauren.sophie.smyth@cern.ch

A Time Dependent Angular Analysis of the Rare Decay $\bar{B}^0_s, B^0_s \to \phi(\to K^+K^-)\mu^+\mu^-$

Lauren Smyth
NMS Summer Student 2024
CERN, CH-1211 Geneva, Switzerland

Keywords: Rare Decays, B-meson Physics, PDFs, Angular Analysis, Time-Dependent Study

Abstract

This report presents both a time-independent and a time-dependent angular analysis study of the rare decay mode $\bar{B}^0_s, B^0_s \to \phi(\to K^+K^-)\mu^+\mu^-$. The time-independent PDF was studied in terms of four CP-averages and four CP-asymmetries of this decay. One-dimensional projections of the helicity angles were plotted and fitted using a maximum-log likelihood fit method. High-statistical toys were generated in order to explore whether the simulated data was unbiased and free from large errors before studying the time-dependent decay scenario. An analytical calculation of the time-dependent PDF was conducted, with a new basis defined analogous to the time-independent case. The time-dependent PDF included new observables with respect to the time-independent case, which could point to a new avenue in which to explore New Physics scenarios. New high-statistical toys were generated and the four one-dimensional projections were plotted and compared to the time-independent results.

Contents

1 An Introduction: B-Meson Physics.

"The scientist does not study nature because it is useful; he studies it because he delights in it, and he delights in it because it is beautiful. If nature were not beautiful, it would not be worth knowing, and if nature were not worth knowing, life would not be worth living."

Henri Poincaré [47].

This report will begin by providing an introduction to the Standard Model of Elementary Particle Physics (SM). This introduction will include explanations of the particles and forces of the SM and their interactions. B-meson physics will be explored next, including CP-violation and B-meson mixing. After this section, the analytical and numerical results of both the time-independent and time-dependent angular analysis of the rare B-meson decay $B_s^0 \to \phi(\to K^+K^-)\mu^+\mu^-$ is reported.

1.1 The Standard Model of Elementary Particle Physics

Particle physics explores the elementary particles of our Universe [1] and how they interact with one another to form the Universe as we know it. The interactions between these

[1]A common misconception is that the elementary particles are the fundamental building blocks of our Universe. In fact, the 'true' building blocks of our Universe are in fact quantum fields [46][51]. There is a corresponding field for each of the twelve particles in the SM. Ripples in these field carry bundles of energy, each of which is what we call a particle. The forces of the SM also have corresponding fields, and work with the fields of particles to create the universe we see today.

constituents are described using, what are known as, the *four fundamental forces*: gravity, the weak nuclear force, hypercharge[2] and the strong nuclear force [45].

The Standard Model (SM) encapsulates our current understanding of particle physics, giving us a picture of the universe in which the forces between particles are themselves described by the exchange of particles. It is the most general quantum field theory of the known particles with $SU(3) \times SU(2) \times U(1)$ symmetry [45]. The fields of $U(1)$ symmetry needed in the SM describe hypercharge, while $SU(3)$ and $SU(2)$ fields correspond to the strong and weak nuclear forces, respectively. As indicated by Figure 1, there are twelve

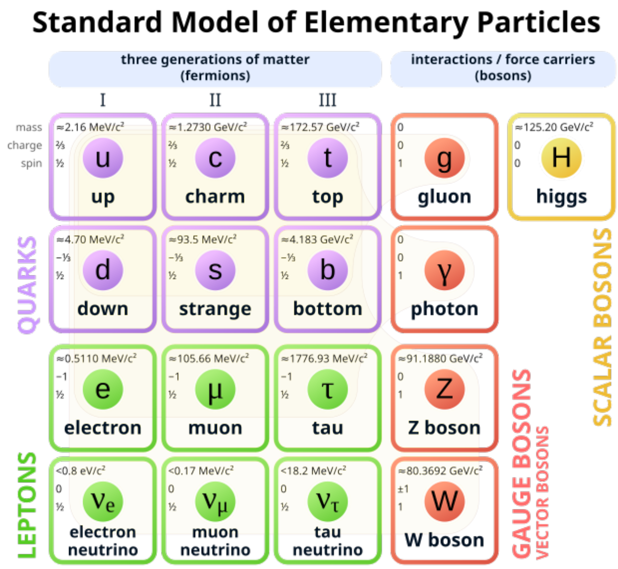

Figure 1: The Standard Model (SM) of Elementary Particles! Image courtesy of Reference [53].

matter particles and five force carrying particles, which are fermions and bosons respectively [3]. The twelve matter particles consist of six quarks and six leptons, all of spin $\frac{1}{2}$ and they are organised by three *generations*. Each generation roughly consists of an electron-like particle, two quarks and a neutrino. Particles from the second and third generations are generally more unstable due to their heavier mass, and subsequently decay into the lighter particles of the first generation [45][48]. While the electrons and the neutrinos can be observed in isolation[4] and are not affected by the strong force, the quarks are special in that they can only be observed hidden within *hadronic* particles.

[2]Another common misconception is that electromagnetism is a fundamental force. While this is usually the case in nature, it should be replaced by *hypercharge* at the fundamental level, i.e., at very short distances.

[3]This is precisely why the Higgs boson is characterised as a force carrying particle, since it has integer intrinsic spin. The Higgs boson is unique in that it is the only fundamental particle which has zero intrinsic spin, making it the simplest particle in the SM [22][34].

[4]Until recently, neutrinos could only be observed indirectly, with the help of momentum conservation [9]. The first direct observation of neutrinos by the FASER detector at the LHC was first reported in 2023 [2].

1.1.1 Quantum Chromodynamics - The Strong Interaction

In essence, quarks are extremely shy! In any decay or collision process, they quickly *hadronise* under the affect of the strong force to form the group of composite particles known as the hadrons. This group segregates into two "families", categorising particles based on their *valence* quark composition. Mesons are composed of a *valence* quark and anti-quark and have integer spin, for example, the B mesons are composed of a bottom anti-quark $\bar{b}$ and either an up u, down d, strange s or charm c quark corresponding to the B^+, B^0, B_s^0 and B_c^+ mesons respectively [50]. On the other hand, baryons consist of favourably three *valence* quarks and have half-integer spin, for example the proton p and neutron n have a valence quark composition uud and udd respectively [45]. You can also verify for yourself the valence quark composition by summing up the charges of the quarks composing a hadron (see Figure 1) and see if they match the charge of that particle ($+\frac{2}{3}+\frac{2}{3}-\frac{1}{3}=+1$ for the $p(uud)$). In the interest of completeness, I must mention the tetraquarks and the pentaquarks. The tetraquark is composed of two valence quarks and antiquarks and has integer spin, hence being classified as an "exotic" meson [38]. The tetraquark $X(3872)$ was detected in 2003 by the Belle experiment [14], being the first of its kind to be observed experimentally. On the other hand, pentaquarks are composed of four valence quarks and one valence antiquark. Due to their odd number of valence quarks and half-integer spin, they are classified as "exotic" baryons. The LHCb reported the first observation of pentaquarks, namely $Pc(4450)^+$ and $Pc(4380)^+$, in 2015 [1].

I have pedantically mentioned the term *valence* when describing the quark composition of the hadrons. However, it is important to note that the quarks are the only constituents of the experimentally observed hadrons. In reality, hadrons consist of a *sea* of equal numbers of quarks and antiquarks of each flavour[5] and *gluons*. Gluons are the spin 1 particle associated with the $SU(3)$ Yang-Mills theory, or the strong interaction [28][21], and their job is to bind or 'glue' the quarks into hadron bound states. Like quarks, they are not observed in isolation but rather via jets [6].

All particles that participate in strong interactions carry the (conserved) quantum number *colour*, of which there are three distinguishable types: red, green and blue [7]. Colour is simply a label for the orthogonal states in the colour space [50], i.e., the non-Abelian gauge group $SU(3)$. Only the particles that have non-zero colour charge couple to the gluons as can be seen in Figure 2, which in this case would be the quarks and the gluon itself! By coupling $SU(3)$ Yang-Mills theory to the quark fields, we now obtain *Quantum Chromodynamics* (QCD): the theory of the strong force [57]. It should be noted that the strength of QCD interaction is independent of the colour charge of the quark, following from the fact that QCD is invariant under unitary transformations in colour space.

1.1.2 The Electroweak Interaction & The Higgs Field

Moving away from the strong interaction, there are four other force-carrying particles besides the gluon. Amongst the *gauge* bosons, the photon is the mediator of the electromagnetic

[5] The flavour of a quark is just its name! There are six flavours as seen in Figure 1

[6] Jets are collimated streams of particles produced in high-energy collisions [45].

[7] This choice of colouring is completely arbitrary. However, I will stick to convention throughout this report.

interaction, whereas the W and Z bosons mediate the weak nuclear interaction. As shown in Figure 2, the photon only interacts with charged particles, clearly characteristic of the electromagnetic interaction and has zero mass due to the gauge invariant nature of the SM .

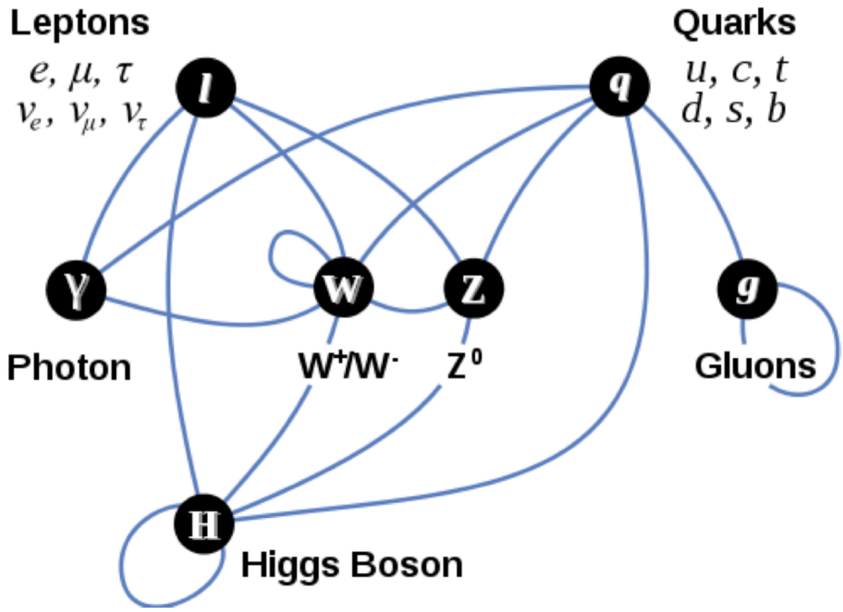

Figure 2: A nice diagram showing which particles of the Standard Model interact interact with one another. A line connecting two particles means that they interact with one another, while a loop indicates that that particle can interact with itself. Full credit for this image goes to Prof Andreas Weiler of TU Munich, taken from his lecture notes of the 'Standard Model' course which he taught during the *CERN Summer Student Lecture Series* in 2024.

The theory of the weak charged-interaction, which is known as $V-A$ theory [27], strongly suggests that the weak interaction is generated by the exchange of a spin 1 boson. The theory, with its current-current interaction, predicted this new boson, the W^-, to carry electric charge of -1, be massive and to have an antiparticle (W^+). There is also a weak neutral-current interaction, closed related to $V - A$ theory, which is mediated by the electrically neutral Z boson. These bosons do not change the type of fermion with which they interact, and $Z-$interactions allow neutrinos to scatter off any other lepton or quark [45].

Before exploring the electroweak theory, we now must come to the *Higgs Boson*. The fundamental particles that we know of obtain their mass via interactions with the *Brout-Englert-Higgs* field [34][22], or more commonly referred to as the *Higgs field*. The Higgs mechanism is how the particles acquire mass without breaking the local gauge symmetry of the SM [45][34]. Consequently, this also includes the Higgs boson itself as it is a massive particle.

A snapshot of how this works can be seen by taking a look at the effective potential shown in Figure 3, given by

$$V(\phi^*\phi) = \mu^2(\phi^*\phi) + \lambda(\phi^*\phi)^2. \tag{1}$$

In this case, ϕ is a complex scalar field and $\mu^2 < 0$ and $\lambda > 0$ are real constants [20]. There is an unstable critical point at the origin where a soon-to-be-massless particle sits. However, this critical point is *unstable* and the particle rolls down to one of the stable minima of the potential well. This choice of settling at a non-zero expectation value of the field $\langle\phi\rangle \neq 0$ causes *spontaneously symmetry breaking*[8] (SSB) of the $SU(2)_L \times U(1)_Y$ global symmetry. This SSB of the Higgs field gives the particles in the SM their masses.

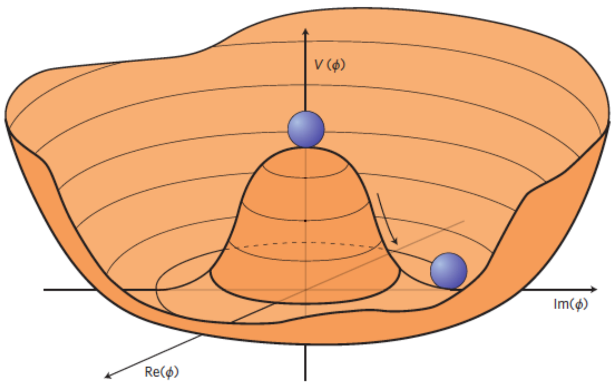

Figure 3: The effective potential of the Higgs field is also known as the "Mexican hat" potential due to its shape. It is precisely because of its shape that the particles in the SM have their mass. Full credit goes to Ref. [20].

The quantum theory for the spin-1 field of a massive particle is the *Glashow-Salam-Weinberg Electroweak Model*, with the gauge group $SU(2) \times U(1)$ defining its underlying structure [30]. This is the model of the unified weak and electromagnetic interactions of the SM, with hypercharge Y being the charge under the $U(1)$ symmetry and the weak isospin quantum number I^a generating the $SU(2)$ gauge symmetry. There is with one vector boson B associated with $U(1)$ (correspond to a phase shift) and three vector bosons A^1, A^2 and A^3 associated with $SU(2)$ (correspond to the rotations around the three axes).

To look into the theory more closely, let's go back to SSB, where I will now introduce *Goldstone's Theorem* [45][31].

Goldstone's Theorem

For every spontaneously broken continuous symmetry, there is a massless particle created by the symmetry current. These particles are known as *Goldstone bosons*.

Let's choose our vacuum state to be [45]

$$\langle\phi\rangle = \begin{pmatrix} 0 \\ \frac{v}{\sqrt{2}} \end{pmatrix}, \qquad v \equiv \sqrt{2}\langle|\phi|\rangle = \frac{\mu}{\sqrt{\lambda}}, \tag{2}$$

with v obviously being related to the minima of the potential well of Equation 1. There is clearly SSB since $v \neq 0$. Expanding around the vacuum state in the complex plane (see Figure 3) gives

[8]In a system with an infinite number of degrees of freedom, there can be several ground states of the Hamiltonian of the system, all with the same energy, such that any one of these states has an orientation with respect to the symmetry transformation. [45]

$$\phi(x) = \begin{pmatrix} H^+(x) \\ \frac{1}{\sqrt{2}}(v + h(x) + iH^0(x)) \end{pmatrix}, \tag{3}$$

where $H^+ = \frac{1}{\sqrt{2}}(H^1(x) + iH^2(x))$ and H^0 are Goldstone bosons and $h(x)$ is the field of the Higgs boson. By a gauge transformation, these Goldstone bosons can be set to zero and by doing so it is said that the vector (gauge) bosons 'eat' the Goldstone bosons and become massive (See Figure 4).

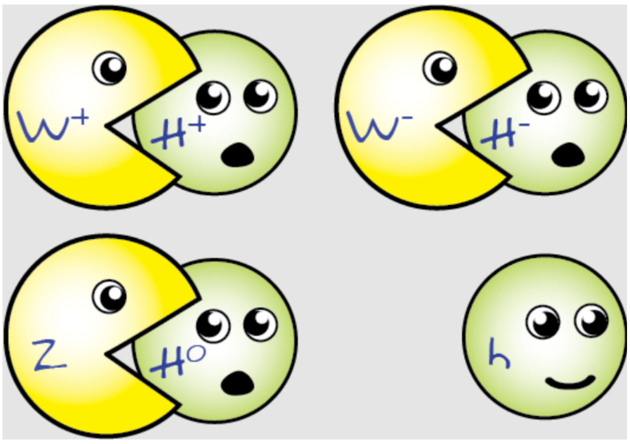

Figure 4: The electroweak vector bosons eating the Goldstone bosons to become massive! Full credit goes to the Quantum Diaries Physics Blog[52].

The kinetic term of the Higgs field can now be constructed with the covariant derivative responsible for coupling the gauge fields A_μ^a and B_μ to any fermions, which on the Higgs field, is given by

$$D_\mu \phi = (\partial_\mu - igA_\mu^a I^a - ig' B_\mu Y) \begin{pmatrix} 0 \\ \frac{v}{\sqrt{2}} \end{pmatrix}. \tag{4}$$

The theory has two coupling constants g ($SU(2)$) and g' ($U(1)$) corresponding to the two independent gauge groups (see Equation 4). However, they are not equal, leading to free parameter $\frac{g'}{g}$ of the theory. Consequently, the weak mixing angle θ_w is defined as

$$\tan\theta_w = \frac{g'}{g}, \tag{5}$$

which is important in expressing the three massive W^+, W^- and Z and one massless vector boson (the photon) in terms of the four vector bosons of the electroweak theory.

After taking the modulus squared of Equation 4 and expanding out the resulting kinetic term, we obtain expressions of the masses of the $W^\pm$ and Z bosons [45][50].

$$m_W = \frac{gv}{2} \qquad m_Z = \sqrt{\frac{(g+g')v}{2}}. \tag{6}$$

The electroweak theory also leaves exactly one vector boson massless, which we can identify as the photon. Also in the electroweak theory, the basic electric charge e is derived from the coupling constants to be [45][30]

$$e = \frac{gg'}{\sqrt{g^2 + g'^2}}. \tag{7}$$

The unification of the weak and electromagnetic interaction between elementary particles is one of the great theoretical advancements in particle physics of the 20$^{\text{th}}$ century. The Nobel Prize of Physics was awarded to Glashow, Salam and Weinberg in 1979 [44], whom the electroweak theory is named after. The W and Z bosons were first directly observed not long after this by the $UA1$ and $UA2$ experiments at CERN in 1983 [5][6].

The Standard Model Lagrangian

Taking all of the above into account, the Lagrangian for the SM is given by

$$\begin{aligned}\mathcal{L}_{\text{SM}} = -\frac{1}{4}\sum_a (F_a^{\mu\nu})^2 + m_W^2 W_\mu^+ W^{-\mu} + \frac{1}{2} m_Z^2 Z_\mu Z^\mu \\ + \sum_f \bar{\Psi}_f (i\gamma^\mu D_{\mu,f} - m_f)\Psi_f + \frac{1}{2}(\partial_\mu h)^2 - V(h),\end{aligned} \tag{8}$$

where a sums over the number of generators of the $SU(3) \times SU(2) \times U(1)$ group and f sums over the number of quark and lepton flavours [45]. The covariant derivatives

$$D_{\mu,f} = \partial_\mu - ieQ_f A_\mu - i\frac{g}{c_w} Q_{Zf} Z_\mu - ig_s A_\mu^a t^a, \tag{9}$$

representing electromagnetic, Z, and gluon couplings to fermions, as well as a $W^\pm$ interaction [45][50].

1.1.3 Possibility for New Physics

Even though it is by far one of the most successful scientific theories of all time, the Standard Model description is incomplete and leaves a lot of unanswered questions. Such problems include the hierarchy problem [4], the strong CP problem [56], neutrino oscillations [15], and more.

So, there are clearly plenty of reasons to search for new physics (NP) and also to test the SM. One such "playground" for such searches is the rare neutral $B-$meson decays mediated by *flavour-changing-neutral-currents* [19]. An angular analysis of new, independent observables for the weak-decays $B_s^0, \bar{B}_s^0 \to \phi(\to K^+K^-)\mu^+\mu^-$ will be the focus of this report. But before I report the findings of the analysis, we need to know a little bit more about the physics of B -meson systems, particularly their *mixing* properties of their decays, potential for *flavour tagging* and how a large number of B-meson processes *violate the CP symmetry.*

1.2 Physics of the B-Meson Systems

As mentioned in Section 1.1, B-mesons are composed of a $\bar{b}$ anti-quark and either a u,d,s or c quark. For processes involving neutral $B-$meson systems, CP violation has been observed

[13]. In discussing CP violation, I will naturally have to talk about *mixing* in this heavy meson systems and the *Cabibbo-Kobayashi-Maskawa* (CKM) matrix. Another interesting property of the $B-$meson system is *flavour-tagging*, since $B-$mesons have a valence b quark in their composition. Such will be the discussion of this section.

1.2.1 CP-Violation

CP violation is *essential* in understanding particle physics. For example, baryogenesis, i.e., the process which caused the domination of matter over anti-matter in the early universe, is explained by this symmetry violation [50][7]. CP violating effects can only be accommodated in the SM within the weak interactions between quarks and leptons [37].

Cabbibo in 1963 came up with a hypothesis stating that the weak interactions of quarks would have the same strength as the leptons, but the weak eigenstates of quarks are *different* from the mass eigenstates [12]. The weak eigenstates are related to the mass eigenstates by a unitary matrix.

In the case of the three quark generations of the SM, this unitary matrix is the *Cabbibo-Kobayashi-Maskawa* (CKM) matrix [37], given by

$$\begin{pmatrix} d' \\ s' \\ b' \end{pmatrix} = \begin{pmatrix} V_{ud} & V_{us} & V_{ub} \\ V_{cd} & V_{cs} & V_{cb} \\ V_{td} & V_{ts} & V_{tb} \end{pmatrix} \begin{pmatrix} d \\ s \\ b. \end{pmatrix} \tag{10}$$

The matrix elements V_{ij} of the CKM matrix given in Equation 10 represent the strength of the flavour changing interaction from a quark of flavour j to a quark of flavour i. The diagonal elements represent the transitions in a given quark generation, with all other off-diagonal elements having the responsibility for the transitions between different generations[9].

The 2×2 sub-matrix located in the upper-left corner of the CKM matrix is the *Cabibbo matrix*

$$\begin{pmatrix} d' \\ s' \end{pmatrix} = \begin{pmatrix} V_{ud} & V_{us} \\ V_{cd} & V_{cs} \end{pmatrix} \begin{pmatrix} d \\ s \end{pmatrix} = \begin{pmatrix} \cos\theta_c & \sin\theta_c \\ -\sin\theta_c & \cos\theta_c \end{pmatrix} \begin{pmatrix} d \\ s \end{pmatrix}, \tag{11}$$

which is a rotation matrix under the *Cabbibo angle* θ_c [12]. So, $SU(2)$ mixes quarks![10].

But how does the CKM matrix help us in the exploration of CP violation? To see this, the *Wolfenstein parameterization* of the CKM matrix becomes extremely useful [55]:

$$V_{CKM} = \begin{pmatrix} 1-\frac{1}{2}\lambda^2 & \lambda & A\lambda^3(\rho - i\eta) \\ -\lambda & 1-\frac{1}{2}\lambda^2 & A\lambda^2 \\ A\lambda^3(1-\rho-i\eta) & -A\lambda^2 & 1 \end{pmatrix} + \mathcal{O}(\lambda^4). \tag{12}$$

Equation 12 is a phenomenological expansion in the powers of $\lambda \equiv |V_{us}| = \sin\theta_c \approx 0.22636$ [11]. I have highlighted the complex phase η because this is the source of CP violation in the CKM matrix. If this irreducible complex phase is *non-zero*, the CP is violated in the quark sector of the SM [55].

[9]see Figure 1 for a reminder on the quark generations

[10]When the experimental measurements for V_{ud} and V_{us} were published, Cabibbo observed that $|V_{ud}|^2 + |V_{us}|^2 = 1$, which in turn inspired this hypothesis [12].

[11]Remember from Equation 11! This shows that the strength of the flavour changing interaction between the up and strange quarks to be small in comparison with the up and down quarks.

Since the experimental measurements of branching ratios do not provide any information about this complex phase [50], measurements sensitive to the amplitudes [12], as opposed to the amplitudes squared are needed. These measurements can be made in neutral kaon and B-meson systems. For this report, I will focus on the latter.

1.2.2 B-meson systems & Mixing

Neutral mesons have the ability to transform via oscillations into their corresponding anti-meson. This quantum mechanical phenomenon is known as *mixing*. This is possible because the CKM matrix is non-diagonal, thus allowing both the quark and anti-quark to transition to another quark flavour. There are two neutral $B^0 - \bar{B}^0$ meson systems, $B_d^0 - \bar{B}_d^0$ and $B_s^0 - \bar{B}_s^0$, which exhibit such mixing [50][45][41]. However, I will focus on the latter system for this section.

An initial state of the $B_s^0 - \bar{B}_s^0$ system must be considered as a superposition of the meson and anti-meson state before it evolves in time. For example,

$$|\mathcal{B}(0)\rangle = b(0)|B_s^0(0)\rangle + \bar{b}(0)|\bar{B}_s^0(0)\rangle \tag{13}$$

describes such an initial state, with $b(0)$ and $\bar{b}(0)$ being the fractions of the initial state being in state $|B_s^0(0)\rangle$ and $|\bar{B}_s^0(0)\rangle$ respectively [45][41][50][24]. The evolution of this state over time can be determined via the time-dependent Schrödinger equation, with an effective Hamiltonian of the system [41][24]

$$H = M - i\Gamma = \begin{pmatrix} M_{11} - i\Gamma_{11} & M_{12} - i\Gamma_{12} \\ M_{21} - i\Gamma_{21} & M_{22} - i\Gamma_{22} \end{pmatrix}. \tag{14}$$

The Hermitian matrices M and Γ in Equation 14 play a physical role in these systems. The matrix Γ is the decay matrix, responsible for representing the decay of the time-dependent state of the system [50][41]. On the other hand, M is the mass matrix, whose diagonal elements are the mass terms for the B_s^0 and B_s^0 *flavour* eigenstates and whose off-diagonal elements correspond to the $B_s^0 \leftrightarrow \bar{B}_s^0$ mixing Feynman diagrams [50][41].

If Equation (14) is a non-diagonal matrix then its eigenstates have well defined masses and widths, but the B_s^0 and $\bar{B}_s^0$ mesons do not since they would not be mass eigenstates [45][50]. The eigenstates of Equation (14) are known as the light and heavy eigenstates, since the mass of the heavy eigenstate m_H is larger than the mass of the light eigenstate m_L of the system.

In the mass eigenbasis, the solution to the eigenvalue problem is simply

$$|B_{s;L,H}^0\rangle = p|B_s^0\rangle \pm q|\bar{B}_s^0\rangle, \tag{15}$$

where the coefficients p and q are normalised by $|p|^2 + |q|^2 = 1$ [36][41]. This normalisation comes from the assumption of CPT symmetry and the fraction of these coefficients is bounded by

[12]In this context, amplitudes refer to the complex quantities associated with the probability of a particular quantum mechanical process, such as a particle decay or a scattering event.

$$\left(\frac{q}{p}\right)^2 = \frac{M_{12}^* - \frac{i}{2}\Gamma_{12}^*}{M_{12} - \frac{i}{2}\Gamma_{12}}. \tag{16}$$

Analysis of the eigenvalues of the eigenstates give the masses and decay widths of the states $|B^0_{s:L,H}\rangle$. For the B^0_s system, the mass, and decay width differences between the light and heavy eigenstates are respectively defined as

$$\Delta m_s = m_H - m_L \qquad \text{and} \qquad \Delta\Gamma_s = \Gamma_L - \Gamma_H. \tag{17}$$

The time-dependent Schrödinger equation must be solved for a time-dependence study of the $B^0_s - \bar{B}^0_s$ system. It is more convenient to solve for the wave functions in terms of the mass eigenstates $B^0_{s:L,H}$ [13] and then use Equation (15) to solve for the time-dependent wave functions for the B^0_s and $\bar{B}^0_s$ mesons. The final results are given by (Full details of this derivation can be found in Reference [41])

$$|B^0_s(t)\rangle = g_+(t)|B^0_s(0)\rangle + \frac{q}{p}g_-(t)|\bar{B}^0_s(0)\rangle, \tag{18}$$

$$|\bar{B}^0_s(t)\rangle = \frac{q}{p}g_-(t)|B^0_s(0)\rangle + g_+(t)|\bar{B}^0_s(0)\rangle, \tag{19}$$

where

$$g_\pm(t) = \frac{1}{2}\left(e^{iM_Lt}e^{-\frac{1}{2}\Gamma_Lt} \pm e^{iM_Ht}e^{-\frac{1}{2}\Gamma_Ht}\right). \tag{20}$$

B-mesons have a special quality in that their processes can be identified or "tagged" within the particle jets produced in high-energy collisions. This is possible due to the relatively long-lifetime of the b-quark in comparison with other quark flavours [50][25]. Knowledge of flavour at production of the B-signal candidate is essential for measurements of CP violation, which is one of the primary tasks set out by the LHCb [25][24]. Although the study of this report look at the un-tagged case in the mode of interest, a nice summary of b-quark tagging can be found in [50].

2 Angular Analysis of a Rare B-meson Decay

This section will provide details about the rare decay $B^0_s \to \phi(\to K^+K^-)\mu^+\mu^-$ studied in this project. This section will also focus on Probability Density Functions (PDF's) and particular observables of interest when looking for potential New Physics (NP) scenarios. This section also endeavours to report on both the time-independent and time-dependent cases in this angular analysis study.

2.1 The Rare Decay - $B^0_s \to \phi(\to K^+K^-)\mu^+\mu^-$

The rare decay $B^0_s \to \phi\mu^+\mu^-$ only occurs at loop level in the SM, mediated by electroweak penguin and box diagrams (see Figure 5). Mathematically speaking, the decay mode can be split up into two different processes: the quark level transition $b \to sl^+l^-$ (see the bottom

[13] Since the Hamiltonian is diagonal in the mass basis

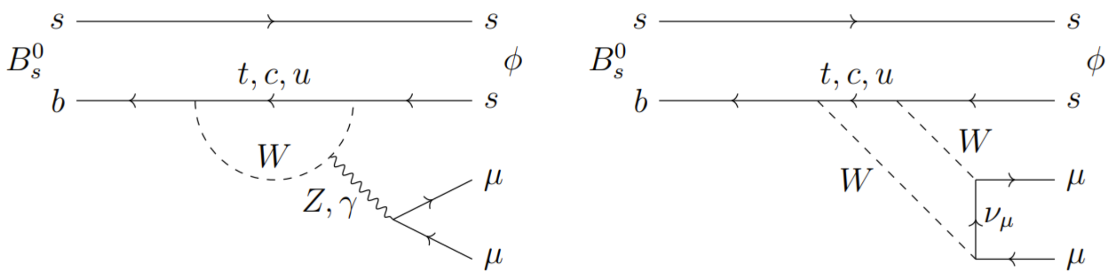

Figure 5: The electroweak penguin (left) and box (right) diagrams which mediate the $B_s^0 \to \phi\mu^+\mu^-$ decay in the SM. Note that the arrows represent the direction of charge. Full credit for this image goes to [41].

part of the electroweak penguin diagram[14] in Figure 5) and the hadronic part of the decay, i.e., the $B_s^0 \to \phi$ transition [41]. The former can be described by an *effective field theory* (EFT) [15], while the later is described using form factors. Given that ϕ is a vector meson with spin 1, i.e., three polarisations, it allows for a rich angular structure (see Section 2.1.2 for more details).

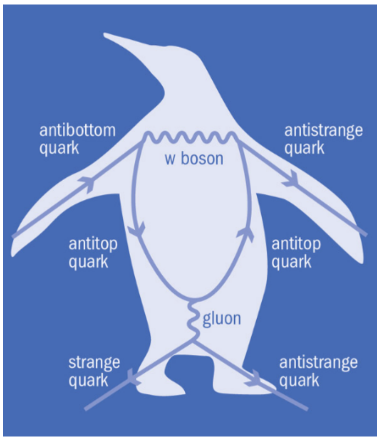

Figure 6: How a Feynman diagram gets a penguin shape! An example of how B_s decays through a loop. Full credit for this image goes to Symmetry/Fermilab/ATLAS [35][26][40].

2.1.1 EFTs, Hadronic Form Factors & New Physics

To start, let's look at EFTs with the quark level transition. EFTs are systematic approximations of a more fundamental underlying theory. EFTs are common and powerful tools in particle physics and allow us to make predictions at experiments like the LHC at CERN and other experiments with multiple energy scales of interest [43]. EFTs use the ratio of these energy scales as an expansion [11].

[14]The name "penguin" diagrams partly came from their shape and partly due to a legendary bet in a bar between Melissa Franklin and John Ellis [49]!

[15]See References [3] and [8] for a more in depth description for this particular quark transition.

A EFT for an arbitrary weak effective theory (WET) decay process can be described with the following effective Hamiltonian

$$\mathcal{H}_{\text{eff}} = \frac{G_F}{\sqrt{2}} \lambda^{\text{CKM}} \sum_i C_i \mathcal{O}_i + h.c., \tag{21}$$

where G_F is the Fermi constant[16], C_i are the *Wilson coefficients* and $\mathcal{O}_i$ are *local* operators [17] [11]. The sum is carried out over all operators allowed by the symmetries of the theory [43]. To describe the transition of the b quark, this expansion, known as the operator product expansion (OPE) is commonly used [19] [18] is commonly used to describe the transition of the b quark.

To probe for new physics (NP), what we are really looking to measure are these Wilson coefficients C_i's. They are essentially coupling constants: encoding all short-range contributions, while also acting as an effective coupling to the local operators (long-range contributions) [42]. They are important as they are used to determine the SM expectation for observables such as branching fractions or angular observables [41]. If NP is present in such decay processes, the values for the Wilson coefficients will naturally be shifted from the SM predicted values.

Physics processes beyond the SM could potentially enter via the Feynman diagrams shown in Figure 5, which in turn, could have large effects on the observables of the decay dependent on the Wilson coefficients [8]. Global fits to all $b \to s\gamma$ and $b \to sll$ data show evidence of tension between theory and experiment [19], including hints at some highly NP scenarios such as the non-universality of lepton flavours [29].

When looking for an EFT, the loop processes of the quark level decay have multiple scales of interest, including the square root of the transferred four momentum ($\sqrt{q^2}$), the energy scale Λ_{QCD} and the masses of the t quark m_t, the $W^{\pm}$ bosons and the mass of the b quark m_b [41]. For the non-mixing case, i.e., where K^+K^- is not necessarily a CP-eigenstate, the EFT Hamiltonian for the quark-level decay $b \to sll$ is simply given by

$$\mathcal{H}_{\text{eff}} = \frac{4G_F}{\sqrt{2}} \left[\lambda_u \mathcal{C}_1 \mathcal{O}_1^u + \lambda_c \mathcal{C}_1 \mathcal{O}_1^c - \lambda_t \sum_{i \in I} \mathcal{C}_i \mathcal{O}_i \right], \tag{22}$$

where $\lambda_q = V_{qv} V_{qs}^*$ and $I = \{3, 4, 5, 6, 8, 7, 7', 9, 9', 10, 10', S, S', P, P', T, T'\}$ [19]. The hadronic operators $\mathcal{O}_J$ where $J \in \{3, 4, 5, 6, 8\}$ are not likely to receive any significant NP contributions [19]. However, the other operators deviate significantly due to NP contributions at the $\mu = m_b$ scale in the SM. The operator $\mathcal{O}_7$ corresponds to a flavour changing neutral current in which a photon is emitted, whereas the operators $\mathcal{O}_{9,10,S,P,T}$ are semi-leptonic operators corresponding to electroweak decays with a vector-, an axialvector-, scalar, pseudoscalar or tensor current, respectively [19] [18][41].

As said previously in Section 2.1, the hadronic transition $B_s^0 \to \phi$ requires the use of form factors and cannot be explained using an EFT. The form factors encapsulate the effects of

[16] Denotes the strength of the interaction

[17] Note that $h.c.$ represents all the hermitian conjugate terms.

[18] The OPE defines the product of fields as a sum over the same fields as an axiom. Under its definition, it offers a non-perturbative approach to QFT. It is a convergent expansion of the product of a finite number of fields at different points as a sum (possibly infinite) of local fields. [54]

the internal structure of the hadrons in the transition, arising from the fact that the hadrons cannot be considered point-like due to their internal quark-gluon structure [46]. There are seven different form factors for the transition under consideration, one for the vector-current, three for the axial-vector currents and three for the tensor currents [41], all depending on the transferred four-momentum q^2. Lattice QCD and the light-cone sum rules (LCSR) are two different approaches one may use to calculate the form factors [33][10]. Both approaches are needed in order to cover the complete q^2 range in an analysis.

2.1.2 Probability Density Functions (PDF's) & Angular Analysis

The time-independent differential decay rate of the decay mode $B_s^0 \to \phi(K^+K^-)\mu^+\mu^-$ is given by

$$
\begin{aligned}
\frac{d^4\Gamma}{dq^2 d\phi d\cos\theta_l d\cos\theta_k} = \frac{9}{32\pi}\Big[& J_{1s}\sin^2\theta_k + J_{1c}\cos^2\theta_k \\
& + J_{2s}\sin^2\theta_k\cos 2\theta_l + J_{2c}\cos^2\theta_k\cos 2\theta_l \\
& + J_3\sin^2\theta_k\sin^2\theta_l\cos 2\phi + J_4\sin 2\theta_k\sin 2\theta_l\cos\phi \\
& + J_5\sin 2\theta_k\sin\theta_l\cos\phi + J_{6s}\sin^2\theta_k\cos\theta_l \\
& + J_7\sin 2\theta_k\sin\theta_l\sin\phi + J_8\sin 2\theta_k\sin 2\theta_l\sin\phi \\
& + J_9\sin^2\theta_k\sin^2\theta_l\sin 2\phi\Big],
\end{aligned} \tag{23}
$$

where J_i are angular coefficients and θ_L, θ_K and ϕ are the helicity angles of the decay [39][23]. These angular coefficients are dependent on the Wilson coefficients and form factors[19] through the transversity amplitudes [19], allowing the exploration for NP. This decay process is described by a set of seven different, complex transversity amplitudes. These represent the different possible polarisation modes of the final state, the chirality of the dimuon system and also the possibility of a spin zero dimuon system configuration [41]. To view how these angular coefficients explicitly depend on the Wilson coefficients, please view References [41] & [19].

In an experimental setting, measuring the momenta and angular distributions of the final-state particles in the decay process leads us to extract the angular coefficients given in Equation (24). The geometric configuration in terms of these helicity angles is given in Figure 7. As shown, the angles θ_L and θ_K are defined as the angles between the B_s^0 and the negatively charged muon and kaon in the dimuon and kaon rest frames respectively. The angle ϕ is the angle between the planes spanned by the dimuon and kaon systems in the B_s^0 rest frame.

Under the approximation where the mass of the muon is small compared to the energy bin ($m_\mu \ll q^2$), J_{1s}, J_{1c} and J_{2s}, J_{2c} [20] are generally not independent and are related by $J_{1s} = 3J_{2s}$ and $J_{1c} = -J_{2c}$ [19]. This can be seen quite explicitly when looking at the angular coefficients presented in References [19] & [41]. The time-independent differential

[19] non-perturbative QCD

[20] Analogous for the $\bar{J}_i's$.

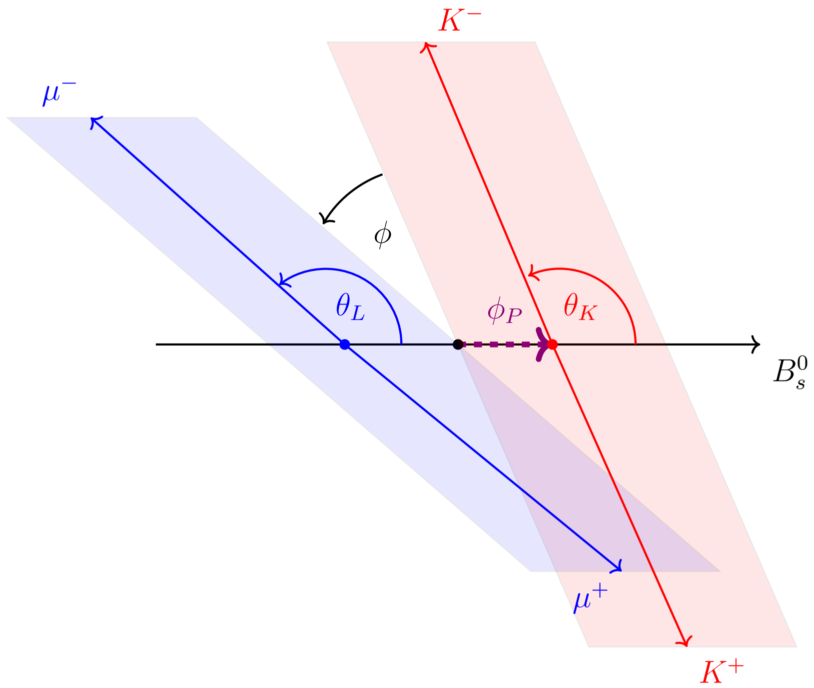

Figure 7: A geometric representation of the $B_s^0 \to \phi(\to K^+K^-)\mu^+\mu^-$ in terms of the helicity angles of the system. Here, the decay product ϕ_P has been labelled with the subscript 'P' in order to differentiate it from the helicity angle ϕ.

decay rate can then be expressed by

$$\begin{aligned}\frac{d^4\Gamma}{dq^2 d\phi d\cos\theta_l d\cos\theta_k} = \frac{9}{32\pi}\Big[& J_{1s}\sin^2\theta_k\left(1+\frac{1}{3}\cos 2\theta_l\right) + J_{1c}\cos^2\theta_k\,(1-\cos 2\theta_l) \\ & + J_3\sin^2\theta_k\sin^2\theta_l\cos 2\phi + J_4\sin 2\theta_k\sin 2\theta_l\cos\phi \\ & + J_5\sin 2\theta_k\sin\theta_l\cos\phi + J_{6s}\sin^2\theta_k\cos\theta_l \\ & + J_7\sin 2\theta_k\sin\theta_l\sin\phi + J_8\sin 2\theta_k\sin 2\theta_l\sin\phi \\ & + J_9\sin^2\theta_k\sin^2\theta_l\sin 2\phi\Big].\end{aligned} \tag{24}$$

Probability density functions[21] (PDFs) of the combined differential decay rate of the $B_s^0 \leftrightarrow \bar{B}_s^0$ were used to model the angular distributions arising from the geometrical interpretation of the decay mode of interest. The PDF for the combined time-independent angular analysis of the $B_s^0 \to \phi(K^+K^-)\mu^+\mu^-$ in terms of CP-averages and CP-asymmetries

[21] A PDF relating a set of independent measurements and physical parameters describes the probability density distribution of events for a given set of values of these physical parameters or for a set of parameters given the measurements [41].

is given by

$$\frac{d^4(\Gamma+\bar{\Gamma})}{dq^2 d\phi d\cos\theta_l d\cos\theta_k}\left(\frac{d(\Gamma+\bar{\Gamma})}{dq^2}\right)^{-1} = \frac{9}{32\pi}\Big[\frac{3}{4}(1-F_L)\sin^2\theta_k\left(1+\frac{1}{3}\cos 2\theta_l\right)$$
$$+ F_L\cos^2\theta_k\,(1-\cos 2\theta_l)$$
$$+ S_3\sin^2\theta_k\sin^2\theta_l\cos 2\phi + S_4\sin 2\theta_k\sin 2\theta_l\cos\phi$$
$$+ A_5\sin 2\theta_k\sin\theta_l\cos\phi$$
$$+ \frac{4}{3}A_{FB}\sin^2\theta_k\cos\theta_l \tag{25}$$
$$+ S_7\sin 2\theta_k\sin\theta_l\sin\phi + A_8\sin 2\theta_k\sin 2\theta_l\sin\phi$$
$$+ A_9\sin^2\theta_k\sin^2\theta_l\sin 2\phi\Big],$$

where $F_L \equiv S_c^1$ is the longitudinal polarisation factor [22] (a CP-average) and $A_{FB} \equiv \frac{3}{4}A_s^6$ is the forward-backward asymmetry (a CP-asymmetry) between the B_s^0 and $\bar{B}_s^0$ meson [41]. As can be observed from Equation (25), CP -averaged observables are represented by the terms $J_{1,2,3,4,7}$ and CP -asymmetric observables by the terms $J_{5,6,8,9}$ [41] and are given by the formulae [41]

$$S_i = J_i + \bar{J}_i \Big/ \frac{d(\Gamma+\bar{\Gamma})}{dq^2} \tag{26}$$

$$A_i = J_i - \bar{J}_i \Big/ \frac{d(\Gamma+\bar{\Gamma})}{dq^2}. \tag{27}$$

With respect to the PDF of Equation (25), the one-dimensional projections of each helicity angle and their fits for the wide q^2 regions $q^2 \in [1.1, 6.0]$ GeV$^2/c^4$ and $q^2 \in [15.0, 18.9]$ GeV$^2/c^4$ are shown in Figures 8-10 and Figures 11-13 respectively in Appendix A.2. The unbinned maximum log-likelihood fit to the toy sample are in good agreement with the data points for each projection in each q^2 bin, showcasing the different characteristics of the system for two different energy ranges. One can clearly see that the minimum and maximum in Figures 8 & 9 for $q^2 \in [1.1, 6.0]$ GeV$^2/c^4$ are more distinct than seen in Figures 11 & 12 for $q^2 \in [15.0, 18.9]$ GeV$^2/c^4$.

The differences in the $\cos\theta_K$ projections (Figures 8 & 11) can be explained by the longitudinal polarisation factor F_L. By looking at the PDF of Equation (25), you notice that the F_L term is proportional to $\cos^2\theta_K$. The value of F_L decreases significantly upon entry into the higher energy band [23] [41], hence for the lower energy band, a more distinct quadratic curve for the $\cos\theta_K$ projection can be observed.

The differences in the $\cos\theta_l$ projections (Figures 9 & 12) are related moreso to the forward-backward asymmetry $A_{\rm FB}$ as well as F_L, whose term in Equation (25) is proportional to $\cos\theta_l$. This is why an approximately linear fit can be seen in Figure 12. For higher F_L

[22] It represents the fraction of decays in which the vector meson, i.e., ϕ in our case, is in the longitudinal polarization state [36].

[23] Helicity suppression and angular momentum conservation favour a longitudinal state at lower energies, but transverse states at higher energies. This can be seen explicitly in the F_L subplot of Figure 9.1 in Reference [41]. This was also seen in the values of F_L generated from the simulated toys in this project.

values in the lower q^2 region, the term proportional to $\cos 2\theta_l$ (and hence $\cos^2\theta_l$) dominates the distribution, making it quadratic. It is also worth noting that the approximation $J_c^1 = -J_c^2$ can be seen from the flipped quadratic distributions of $\cos\theta_k$ and $\cos\theta_l$ for the lower q^2 band with respect to one another.

For the q^2 range $q^2 \in [1.1, 6.0]$ GeV$^2/c^4$, over one-hundred toy data sets were generated to statistically analyse the CP-averages and CP-asymmetries. This was done to check whether the toys were generating as expected with no biases or unexpected errors in order to move the analysis to a time-dependent regime. The distributions of the spread of each observable obtained from the fit with respect to the initial value that was used for its generation and pull for each observable obtained from the fit were plotted and can be seen in Figures 14 and 15 respectively.

The spread helps estimate the uncertainty associated with the measured observable in real data by analysing the variability observed in the toy simulations. It was calculated for each observable as

$$\text{Spread} = \mathcal{O}_i^{\text{fit.}} - \mathcal{O}_i^{\text{gen.}}, \tag{28}$$

for the mean of an observable of the fit $\mathcal{O}_i^{\text{fit.}}$ and the corresponding generated observable $\mathcal{O}_i^{\text{gen.}}$. The spread for each observable fits to a normal Gaussian with mean 0.0 and standard deviation of 0.1[24], indicating consistency of the data.

The pull is a normalized measure of the deviation of an observed data point from the expected value, i.e.,

$$\text{Pull} = \frac{\mathcal{O}_i^{\text{fit.}} - \mathcal{O}_i^{\text{gen.}}}{\sigma_i^{\text{fit}}}, \tag{29}$$

for the mean of an observable of the fit $\mathcal{O}_i^{\text{fit.}}$, the corresponding generated observable $\mathcal{O}_i^{\text{gen.}}$ and the standard deviation of the fit [16]. As can be seen in Figure 15, the pulls for each observable correspond to a normal Gaussian under the fitting framework. The mean of these pulls is zero within the calculated uncertainty, indicating that there is no bias, and the width of the pulls is one within the calculated uncertainty, indicating that the error is correct.

2.2 Angular Analysis of the Time-Dependent PDF

In this section, we move from the time-independent to the time-dependent regime. An analytical calculation for the time-dependent PDF is carried out, with a change of basis in the angular coefficients analogous to that seen in Section 2.1.2. Next, an explanation of the graphical and numerical results with respect to this new PDF will be provided.

2.2.1 Analytical Calculation of the Time-Dependent PDF

The combined untagged angular decay rate can be made explicitly time-dependent by using the following relations [19]

$$J_i(t) \pm \bar{J}_i(t) = e^{-\Gamma t}\left[(J_i \pm \bar{J}_i)\cosh(y\Gamma t) - h_i \sinh(y\Gamma t)\right] \tag{30}$$

where $x \equiv \frac{\Delta m}{\Gamma}, y \equiv \frac{\Delta\Gamma}{2\Gamma}$, and h_i are a new set of angular coefficients related to the time-dependent angular distribution and are expressed in terms in helicitly amplitudes [19][18].

[24]With the exception of F_L having a standard deviation of 0.2.

These new observables are another tool which can be used in the exploration for NP contributions.

In any q^2 region, the combined untagged time-dependent angular decay rate of the B_s^0 and $\bar{B}_s^0$ mesons is given by

$$\begin{aligned}
\frac{d^5(\Gamma+\bar{\Gamma})}{dq^2 d\phi d\cos\theta_l d\cos\theta_k dt} = \frac{9}{32\pi}\Gamma e^{-\Gamma t}\Big[&((J_{1s}+\bar{J}_{1s})\cosh(y\Gamma t) - h_{1s}\sinh(y\Gamma t))\sin^2\theta_k \\
&+ ((J_{1c}+\bar{J}_{1c})\cosh(y\Gamma t) - h_{1c}\sinh(y\Gamma t))\cos^2\theta_k \\
&+ ((J_{2s}+\bar{J}_{2s})\cosh(y\Gamma t) - h_{2s}\sinh(y\Gamma t))\sin^2\theta_k\cos 2\theta_l \\
&+ ((J_{2c}+\bar{J}_{2c})\cosh(y\Gamma t) - h_{2c}\sinh(y\Gamma t))\cos^2\theta_k\cos 2\theta_l \\
&+ ((J_{3}+\bar{J}_{3})\cosh(y\Gamma t) - h_{3}\sinh(y\Gamma t))\sin^2\theta_k\sin^2\theta_l\cos 2\phi \\
&+ ((J_{4}+\bar{J}_{4})\cosh(y\Gamma t) - h_{4}\sinh(y\Gamma t))\sin 2\theta_k\sin 2\theta_l\cos\phi \\
&+ ((J_{5}-\bar{J}_{5})\cosh(y\Gamma t) - h_{5}\sinh(y\Gamma t))\sin 2\theta_k\sin\theta_l\cos\phi \\
&+ ((J_{6s}-\bar{J}_{6s})\cosh(y\Gamma t) - h_{6s}\sinh(y\Gamma t))\sin^2\theta_k\cos\theta_l \qquad (31) \\
&+ ((J_{7}+\bar{J}_{7})\cosh(y\Gamma t) - h_{7}\sinh(y\Gamma t))\sin 2\theta_k\sin\theta_l\sin\phi \\
&+ ((J_{8}-\bar{J}_{8})\cosh(y\Gamma t) - h_{8}\sinh(y\Gamma t))\sin 2\theta_k\sin 2\theta_l\sin\phi \\
&+ ((J_{9}-\bar{J}_{9})\cosh(y\Gamma t) - h_{9}\sinh(y\Gamma t))\sin^2\theta_k\sin^2\theta_l\sin 2\phi\Big].
\end{aligned}$$

When integrated over the angular terms and time, Equation (31) becomes (See A.1 for further details)

$$\begin{aligned}
\left\langle\frac{d(\Gamma+\bar{\Gamma})}{dq^2}\right\rangle = \frac{1}{1-y^2}\Big(&\frac{3}{4}(2(J_{1s}+\bar{J}_{1s}-yh_{1s}) + J_{1c}+\bar{J}_{1c}-yh_{1c}) \\
&-\frac{1}{4}(2(J_{2s}+\bar{J}_{2s}-yh_{2s}) + J_{2c}+\bar{J}_{2c}-yh_{2c})\Big).
\end{aligned} \qquad (32)$$

Under the approximation $m_\mu \ll q^2$ as described in Section 2.1.2, Equation (32) simplifies to

$$\left\langle\frac{d(\Gamma+\bar{\Gamma})}{dq^2}\right\rangle = \frac{1}{1-y^2}\left[\frac{4}{3}(J_{1s}+\bar{J}_{1s}-yh_{1s}) + J_{1c}+\bar{J}_{1c}-yh_{1c}\right]. \qquad (33)$$

Then for

$$\mathrm{PDF} \equiv \frac{d^5(\Gamma+\bar{\Gamma})}{dq^2 d\phi d\cos\theta_l d\cos\theta_k dt}\left\langle\frac{d(\Gamma+\bar{\Gamma})}{dq^2}\right\rangle^{-1},$$

the following expression is the combined time-dependent PDF in terms of the J_i-angular coefficients under the same approximation

$$
\begin{aligned}
\text{PDF} = \frac{9}{32\pi}\left\langle \frac{d(\Gamma+\bar{\Gamma})}{dq^2} \right\rangle^{-1} \Gamma e^{-\Gamma t}\Big[& ((J_{1s}+\bar{J}_{1s})\cosh(y\Gamma t) - h_{1s}\sinh(y\Gamma t))\sin^2\theta_k\left(1+\frac{1}{3}\cos 2\theta_l\right) \\
& + ((J_{1c}+\bar{J}_{1c})\cosh(y\Gamma t) - h_{1c}\sinh(y\Gamma t))\cos^2\theta_k\,(1-\cos 2\theta_l) \\
& + ((J_{3}+\bar{J}_{3})\cosh(y\Gamma t) - h_{3}\sinh(y\Gamma t))\sin^2\theta_k\sin^2\theta_l\cos 2\phi \\
& + ((J_{4}+\bar{J}_{4})\cosh(y\Gamma t) - h_{4}\sinh(y\Gamma t))\sin 2\theta_k\sin 2\theta_l\cos\phi \\
& + ((J_{5}-\bar{J}_{5})\cosh(y\Gamma t) - h_{5}\sinh(y\Gamma t))\sin 2\theta_k\sin\theta_l\cos\phi \\
& + ((J_{6s}-\bar{J}_{6s})\cosh(y\Gamma t) - h_{6s}\sinh(y\Gamma t))\sin^2\theta_k\cos\theta_l \\
& + ((J_{7}+\bar{J}_{7})\cosh(y\Gamma t) - h_{7}\sinh(y\Gamma t))\sin 2\theta_k\sin\theta_l\sin\phi \\
& + ((J_{8}-\bar{J}_{8})\cosh(y\Gamma t) - h_{8}\sinh(y\Gamma t))\sin 2\theta_k\sin 2\theta_l\sin\phi \\
& + ((J_{9}-\bar{J}_{9})\cosh(y\Gamma t) - h_{9}\sinh(y\Gamma t))\sin^2\theta_k\sin^2\theta_l\sin 2\phi\Big],
\end{aligned} \tag{34}
$$

where Equation (33) acts as the normalisation coefficient for the PDF. The basis

$$
\mathcal{K}_i = \frac{J_i+\bar{J}_i}{\langle\mathcal{I}\rangle}, \qquad \mathcal{W}_i = \frac{J_i-\bar{J}_i}{\langle\mathcal{I}\rangle} \qquad \mathcal{H}_i = \frac{h_i}{\langle\mathcal{I}\rangle}, \tag{35}
$$

where

$$
\langle\mathcal{I}\rangle = \frac{4}{3}(J_{1s}+\bar{J}_{1s}-yh_{1s}) + J_{1s}+\bar{J}_{1s}-yh_{1s}, \tag{36}
$$

was used to tidy up Equation (34).

The time-dependent PDF under this basis is

$$
\begin{aligned}
\text{PDF} = \frac{9}{32\pi}\Gamma(1-y^2)e^{-\Gamma t}\Big[& (\mathcal{K}_{1s}\cosh(y\Gamma t) - \mathcal{H}_{1s}\sinh(y\Gamma t))\sin^2\theta_k\left(1+\frac{1}{3}\cos 2\theta_l\right) \\
& + (\mathcal{K}_{1c}\cosh(y\Gamma t) - \mathcal{H}_{1c}\sinh(y\Gamma t))\cos^2\theta_k\,(1-\cos 2\theta_l) \\
& + (\mathcal{K}_{3}\cosh(y\Gamma t) - \mathcal{H}_{3}\sinh(y\Gamma t))\sin^2\theta_k\sin^2\theta_l\cos 2\phi \\
& + (\mathcal{K}_{4}\cosh(y\Gamma t) - \mathcal{H}_{4}\sinh(y\Gamma t))\sin 2\theta_k\sin 2\theta_l\cos\phi \\
& + (\mathcal{W}_{5}\cosh(y\Gamma t) - \mathcal{H}_{5}\sinh(y\Gamma t))\sin 2\theta_k\sin\theta_l\cos\phi \\
& + (\mathcal{W}_{6s}\cosh(y\Gamma t) - \mathcal{H}_{6s}\sinh(y\Gamma t))\sin^2\theta_k\cos\theta_l \\
& + (\mathcal{K}_{7}\cosh(y\Gamma t) - \mathcal{H}_{7}\sinh(y\Gamma t))\sin 2\theta_k\sin\theta_l\sin\phi \\
& + (\mathcal{W}_{8}\cosh(y\Gamma t) - \mathcal{H}_{8}\sinh(y\Gamma t))\sin 2\theta_k\sin 2\theta_l\sin\phi \\
& + (\mathcal{W}_{9}\cosh(y\Gamma t) - \mathcal{H}_{9}\sinh(y\Gamma t))\sin^2\theta_k\sin^2\theta_l\sin 2\phi\Big].
\end{aligned} \tag{37}
$$

The time-independent basis presented in Section 2.1.2 in terms of CP-averages and -asymmetries can be recovered by noting that

$$
S_i = \mathcal{K}_i - y\mathcal{H}_i \qquad A_i = \mathcal{W}_i - y\mathcal{H}_i, \tag{38}
$$

when $y = 0$. Setting $y = 0$ to recover the time-independent results is valid given that $\Gamma_L = \Gamma_H$ when there is no mixing. We can also use Equation (36) to remove one less $\mathcal{K}$ from

Equation (40):

$$
\begin{aligned}
\implies \langle \mathcal{I} \rangle &= \frac{4}{3}(J_{1s} + \bar{J}_{1s} - yh_{1s}) + J_{1s} + \bar{J}_{1s} - yh_{1s} \\
\implies \quad 1 &= \frac{4}{3}(\mathcal{K}_{1s} - y\mathcal{H}_{1s}) + \mathcal{K}_{1c} - y\mathcal{H}_{1c} \\
\implies \mathcal{K}_{1s} &= \frac{3}{4}\left(1 - \mathcal{K}_{1c} + y\left(\frac{4}{3}\mathcal{H}_{1s} + \mathcal{H}_{1c}\right)\right).
\end{aligned} \tag{39}
$$

Hence, Equation (40) simplifies to become the final PDF used in the analysis.

Time-Dependent PDF for the $B_s^0 \to \phi(K^+K^-)\mu^+\mu^-$ Analysis

$$
\begin{aligned}
\text{PDF} = \mathcal{F}(t)\Big[&\left(\frac{3}{4}(1-\mathcal{K}_{1c})\cosh(y\Gamma t) - \mathcal{H}_{1s}\sinh(y\Gamma t)\right)\sin^2\theta_k\left(1+\frac{1}{3}\cos 2\theta_l\right) \\
&+ (\mathcal{K}_{1c}\cosh(y\Gamma t) - \mathcal{H}_{1c}\sinh(y\Gamma t))\cos^2\theta_k\,(1-\cos 2\theta_l) \\
&+ (\mathcal{K}_3\cosh(y\Gamma t) - \mathcal{H}_3\sinh(y\Gamma t))\sin^2\theta_k\sin^2\theta_l\cos 2\phi \\
&+ (\mathcal{K}_4\cosh(y\Gamma t) - \mathcal{H}_4\sinh(y\Gamma t))\sin 2\theta_k\sin 2\theta_l\cos\phi \\
&+ (\mathcal{W}_5\cosh(y\Gamma t) - \mathcal{H}_5\sinh(y\Gamma t))\sin 2\theta_k\sin\theta_l\cos\phi \\
&+ (\mathcal{W}_{6s}\cosh(y\Gamma t) - \mathcal{H}_{6s}\sinh(y\Gamma t))\sin^2\theta_k\cos\theta_l \\
&+ (\mathcal{K}_7\cosh(y\Gamma t) - \mathcal{H}_7\sinh(y\Gamma t))\sin 2\theta_k\sin\theta_l\sin\phi \\
&+ (\mathcal{W}_8\cosh(y\Gamma t) - \mathcal{H}_8\sinh(y\Gamma t))\sin 2\theta_k\sin 2\theta_l\sin\phi \\
&+ (\mathcal{W}_9\cosh(y\Gamma t) - \mathcal{H}_9\sinh(y\Gamma t))\sin^2\theta_k\sin^2\theta_l\sin 2\phi \\
&+ y\left(\frac{4}{3}\mathcal{H}_{1s} + \mathcal{H}_{1c}\right)\cosh(y\Gamma t)\sin^2\theta_k\left(1+\frac{1}{3}\cos 2\theta_l\right)\Big],
\end{aligned} \tag{40}
$$

where

$$
\mathcal{F}(t) = \frac{9}{32\pi}\Gamma(1-y^2)e^{-\Gamma t}. \tag{41}
$$

2.2.2 Results & Analysis of the Time-Dependent PDF

Section A.4 shows the plots used to compared the time-independent projections analysed Section 2.1.2 with the time-dependent projections of the helicity angles in the presence of mixing. In comparison with the time-independent cases, the data distributions for $\cos\theta_k$ and $\cos\theta_l$ in Figures 16 and 17 seem to have more pronounced quadratic curves by observation. A deviation in the shape of the distribution of the ϕ projection can be seen in Figure 21.

Section A.5 shows comparison plots between the mixing and non-mixing cases in the time-dependent study. For the time projections shown in Figure 22, the exponential decay drops off quicker in the mixing case. In the case of the $\cos\theta_k$ projections, the projection is shifted upwards in the mixing case in comparison to the non-mixing case (Figure 19), whereas the quadratic shape to the data of Figure 20 seems to be flattened in the mixing case for the $\cos\theta_l$ projections.

For the plots in Sections A.4 & A.5, the values for Γ and $\Delta\Gamma$ were taken from Reference [32].

3 Conclusions

In this report, the successful generation of statistical toys in both the time-independent and time-dependent cases of the rare decay mode $\bar{B}_s^0, B_s^0 \to \phi(\to K^+K^-)\mu^+\mu^-$ was achieved, with good fitting and statistical results for the time-independent PDF. The investigation included both time-independent and time-dependent probability density functions (PDFs), examined in various bases for the observables under study: the J-basis and the basis in terms of four CP-averages and -asymmetries.

Through one-dimensional projections of helicity angles across different q^2 ranges, it was confirmed that the statistical toys and fits were robust, free from bias, and exhibited minimal statistical errors. Specifically, the spread and pull of each angular observable were consistent with expectations, showing a mean of zero and standard deviations of 0.1 and 1, respectively.

In the time-dependent analysis, the analytic derivation of the time-dependent PDF in the J basis and introduced a new notation to approximate the CP-averages/asymmetries basis used in the time-independent case. This analysis included additional observables, h_i, arising from this time-dependent, which provide another new way for exploring NP. The study also involved simulations to compare mixing and non-mixing scenarios, noting discrepancies between time-independent and time-dependent analyses, as well as between mixing and non-mixing cases.

Looking forward, further extensions to this project are can be considered. Specifically, the fitting framework for the projections needs refinement to ensure accurate and effective analysis. Future work could aim to apply similar analytical methods as in the time-independent case, in order to enhance understanding of NP and its manifestations in rare decays.

Acknowledgements

I would like to thank my supervisors, Dr Michele Atzeni and Prof Eluned Smith, for allowing me to participate in this research project and for their invaluable guidance, support, and encouragement as mentors this summer. I would also like to express my sincere appreciation to the CERN Summer Student Program for providing me with the opportunity to experience the enriching work environment here at CERN. The experience has been both educational and inspiring, and I am thankful for the support and resources provided. Additionally, I am grateful to the CERN & Society Foundation for funding my work, which made my stay at CERN possible as a Non-Member State student.

A Appendix

A.1 Time-Integrated Observables at a Hadron Collider

The explicit calculation of $\langle J_i \pm \bar{J}_i \rangle$ needed to obtain Equation (32) in Section 2.2 is as follows:

$$
\begin{aligned}
\langle J_i \pm \bar{J}_i \rangle &= \int_0^\infty e^{-\Gamma t} \left((J_i \pm \bar{J}_i) \cosh(y\Gamma t) - h_i \sinh(y\Gamma t) \right) \\
&= \int_0^\infty \left(\frac{1}{2}(J_i \pm \bar{J}_i) \left(e^{(y-1)\Gamma t} + e^{-(y+1)\Gamma t} \right) - \frac{1}{2} h_i \left(e^{(y-1)\Gamma t} - e^{-(y+1)\Gamma t} \right) \right) \\
&= \Big|_0^\infty \frac{1}{2\Gamma} \left((J_i \pm \bar{J}_i) \left(\frac{e^{(y-1)\Gamma t}}{y-1} - \frac{e^{-(y+1)\Gamma t}}{y+1} \right) - h_i \left(\frac{e^{(y-1)\Gamma t}}{y-1} + \frac{e^{-(y+1)\Gamma t}}{y+1} \right) \right) \\
&= \frac{1}{2\Gamma} \left((J_i \pm \bar{J}_i) \left(\frac{1}{y-1} - \frac{1}{y+1} \right) - h_i \left(\frac{1}{y-1} + \frac{1}{y+1} \right) \right) \\
&= \frac{1}{\Gamma(1-y^2)} \left[(J_i \pm \bar{J}_i) - h_i y \right]
\end{aligned}
$$

These are the time-integrated observables which can be measured typically somewhere where $\bar{b}b$ quark pairs are incoherently produced, such as a hadron collider [19][18][17].

A.2 Time Independent One-Dimensional Projections of the Helicity Angles

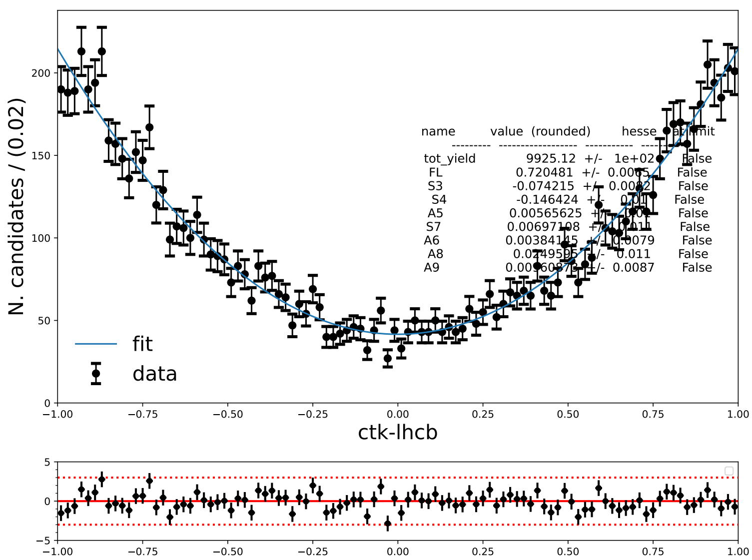

Figure 8: Distribution of $\cos\theta_K$ for $q^2 \in [1.1, 6.0]\text{GeV}^2/c^4$ for the decay (data points) with the one-dimensional projections of the PDF at the maximal likelihood point (blue curve).

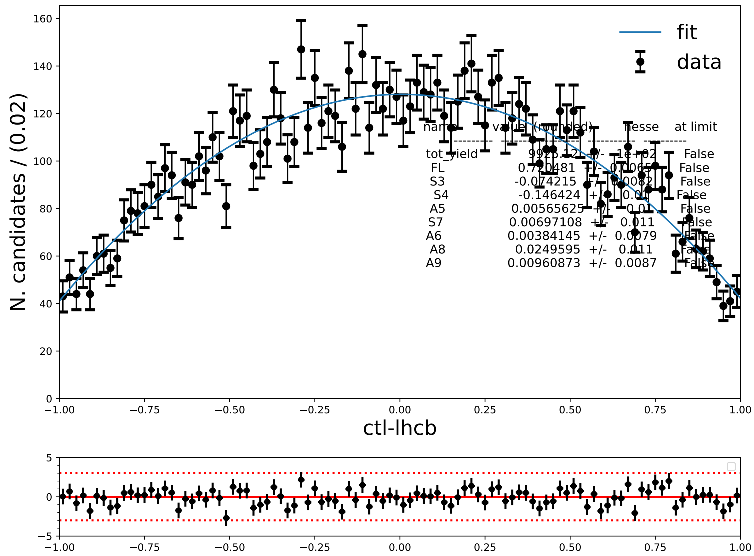

Figure 9: Distribution of $\cos\theta_L$ for $q^2 \in [1.1, 6.0]\mathrm{GeV}^2/c^4$ for the decay (data points) with the one-dimensional projections of the PDF at the maximal likelihood point (blue curve).

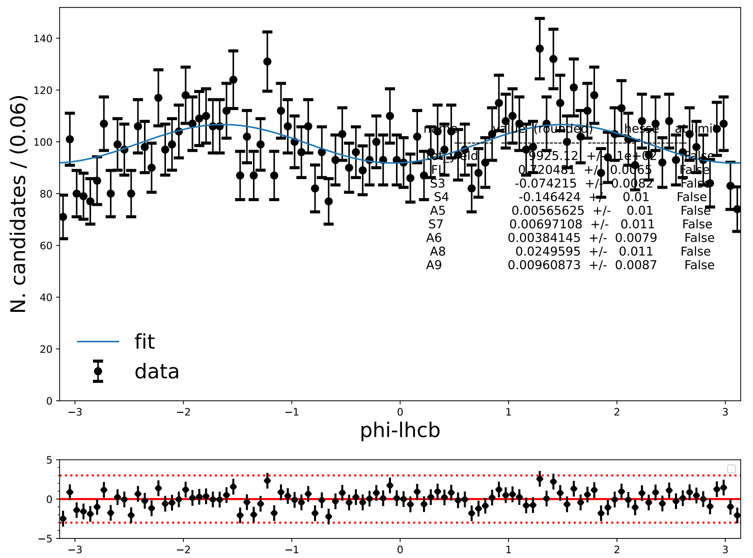

Figure 10: Distribution of ϕ for $q^2 \in [1.1, 6.0]\mathrm{GeV}^2/c^4$ for the decay (data points) with the one-dimensional projections of the PDF at the maximal likelihood point (blue curve).

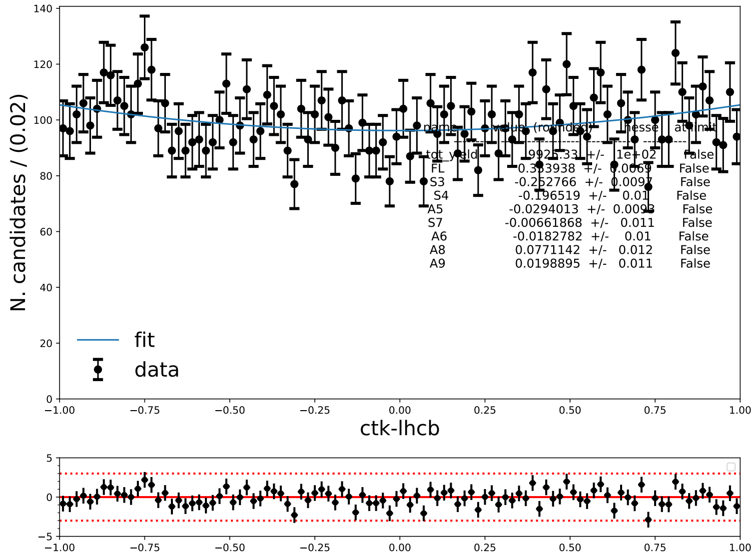

Figure 11: Distribution of $\cos\theta_K$ for $q^2 \in [15.0, 18.9]\mathrm{GeV}^2/c^4$ for the decay (data points) with the one-dimensional projections of the PDF at the maximal likelihood point (blue curve).

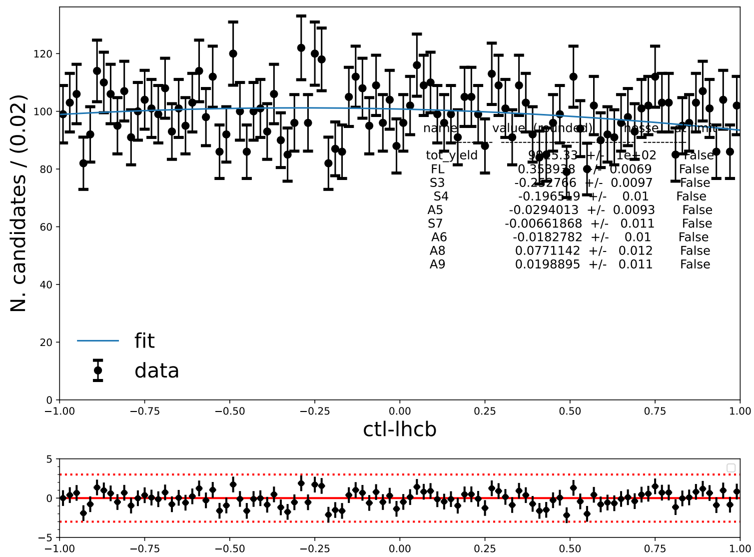

Figure 12: Distribution of $\cos\theta_L$ for $q^2 \in [15.0, 18.9]\mathrm{GeV}^2/c^4$ for the decay (data points) with the one-dimensional projections of the PDF at the maximal likelihood point (blue curve).

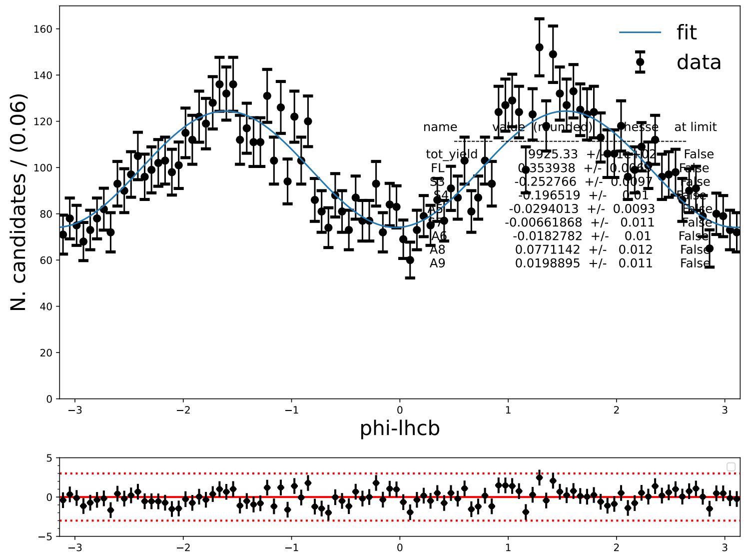

Figure 13: Distribution of ϕ for $q^2 \in [15.0, 18.9]\mathrm{GeV}^2/c^4$ for the decay (data points) with the one-dimensional projections of the PDF at the maximal likelihood point (blue curve).

A.3 Spread & Pull Plots in the Time-Independent Study

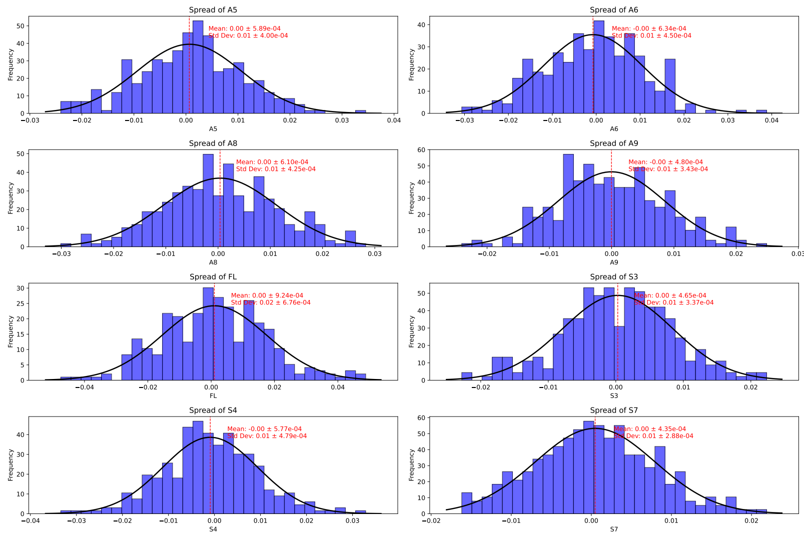

Figure 14: The spread of the observables in the CP-averages and -asymmetries basis from the time-independent angular analysis.

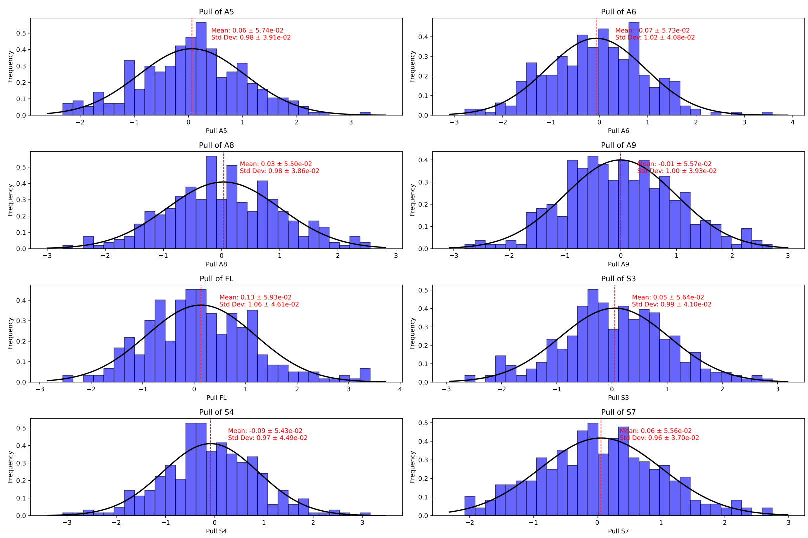

Figure 15: The pull of the observables in the CP-averages and -asymmetries basis from the time-independent angular analysis.

A.4 Time-Independent & -Dependent One-Dimensional Projections of the Helicity Angles

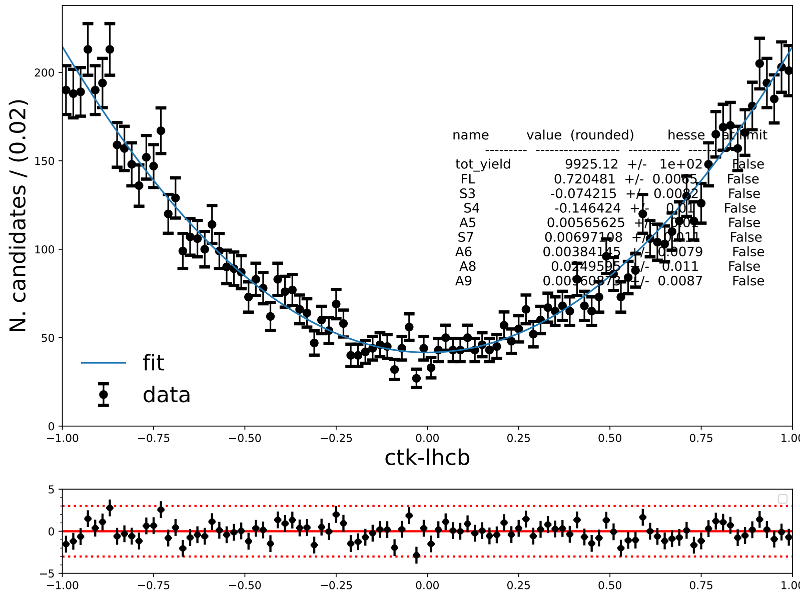

((a)) $\cos\theta_k$ - time independent projection

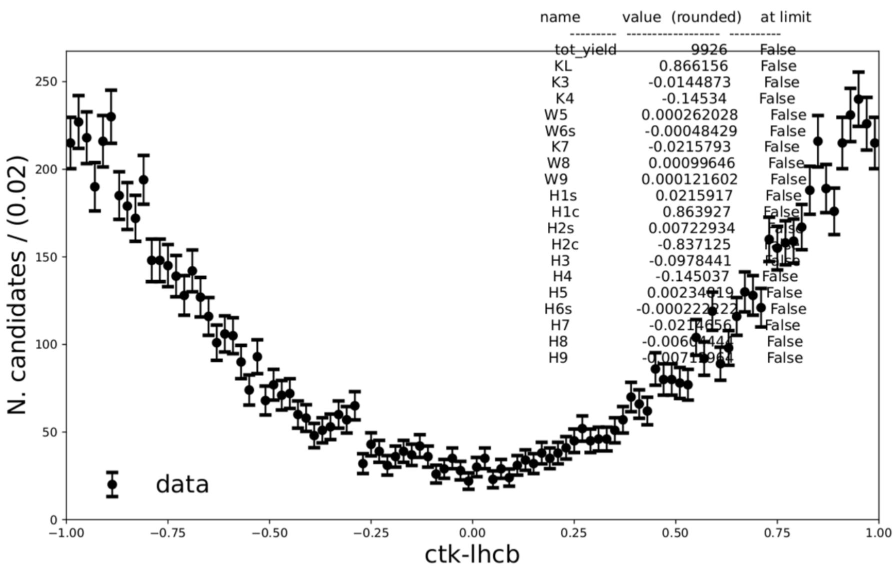

((b)) $\cos\theta_k$ - time dependent projection with mixing.

Figure 16: Time-independent vs. dependent projections of $\cos\theta_k$

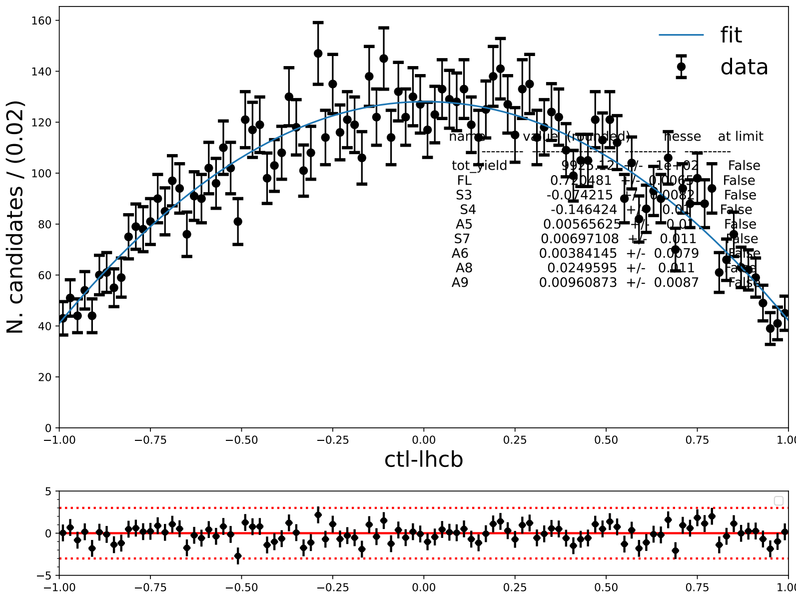

((a)) $\cos\theta_l$ - time independent projection

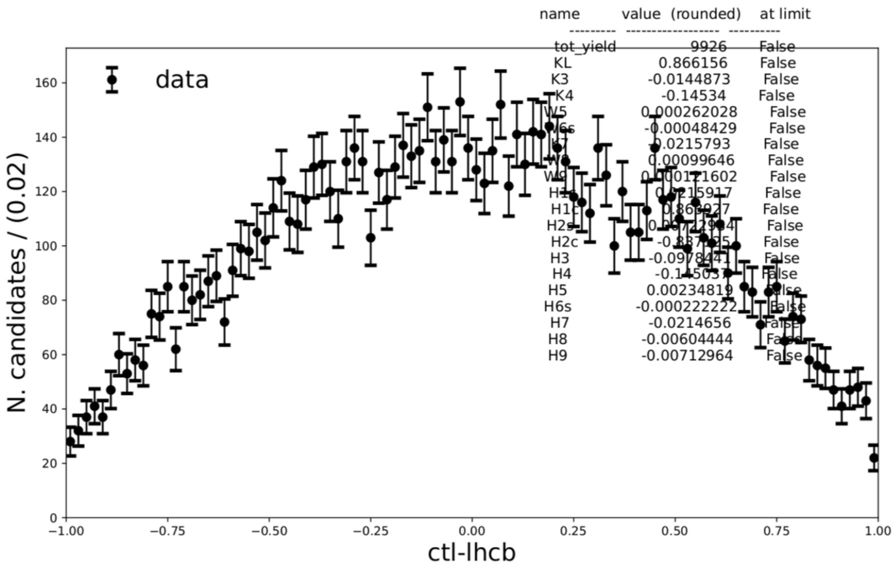

((b)) $\cos\theta_l$ - time dependent projection with mixing.

Figure 17: Time-independent vs. dependent projections of $\cos\theta_l$

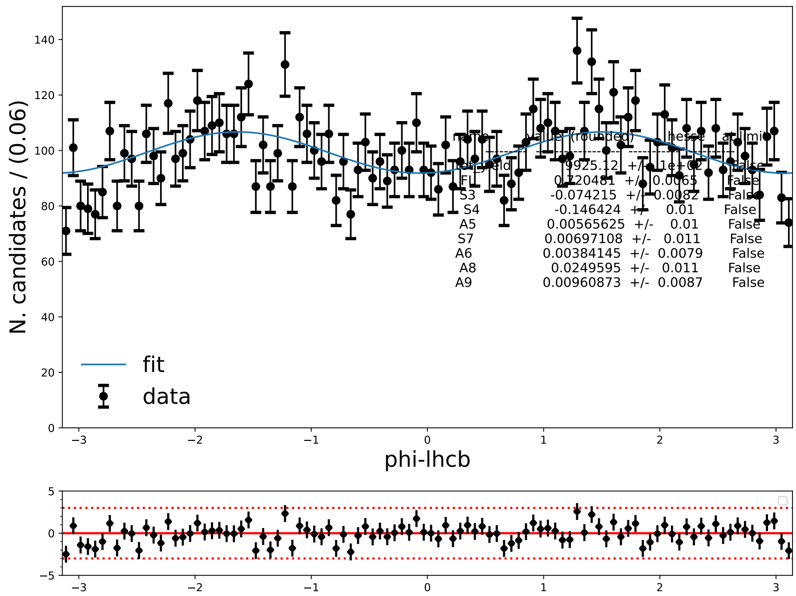

((a)) ϕ - time independent projection

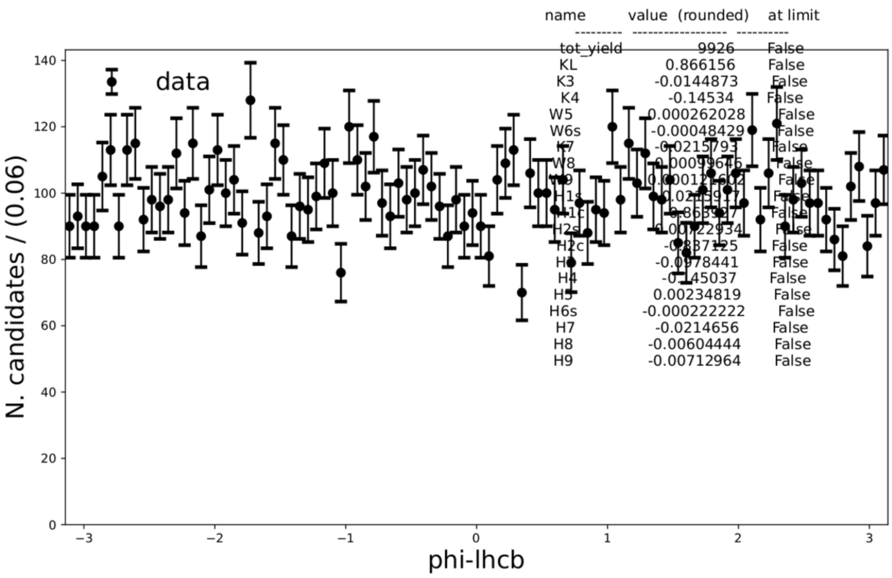

((b)) ϕ - time dependent projection with mixing

Figure 18: Time-independent vs. dependent projections of ϕ

A.5 Time-Dependent One-Dimensional Projections: Mixing ($y \neq 0$) vs. Non-Mixing ($y = 0$)

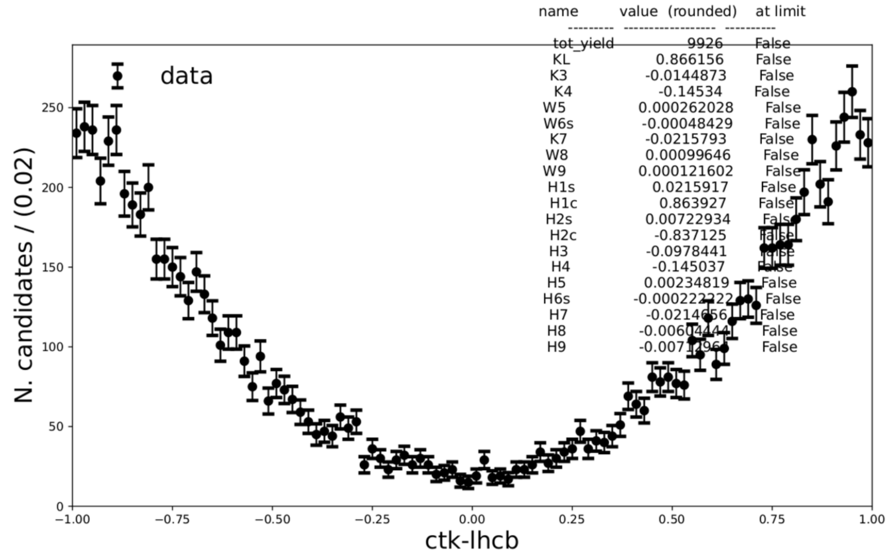

((a)) $\cos\theta_k$ - projection with no mixing, i.e., $y = 0$.

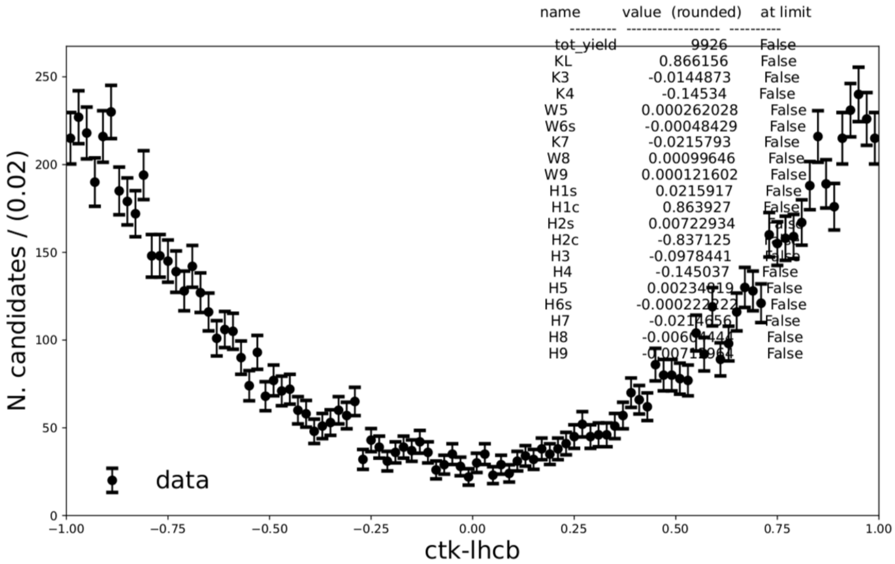

((b)) $\cos\theta_k$ - projection with mixing, i.e., $y \neq 0$..

Figure 19: Mixing vs. Non-Mixing projections of $\cos\theta_k$

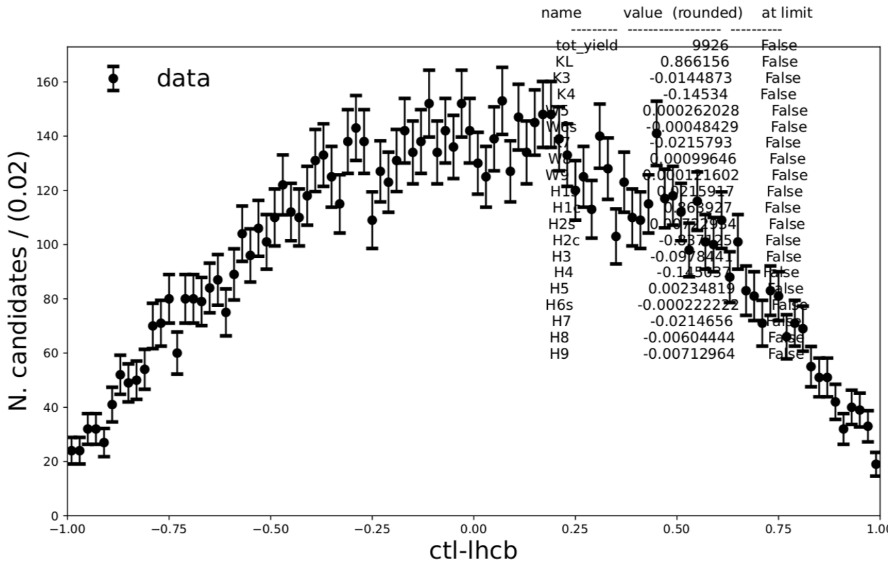

((a)) $\cos\theta_l$ - projection with no mixing, i.e., $y = 0$..

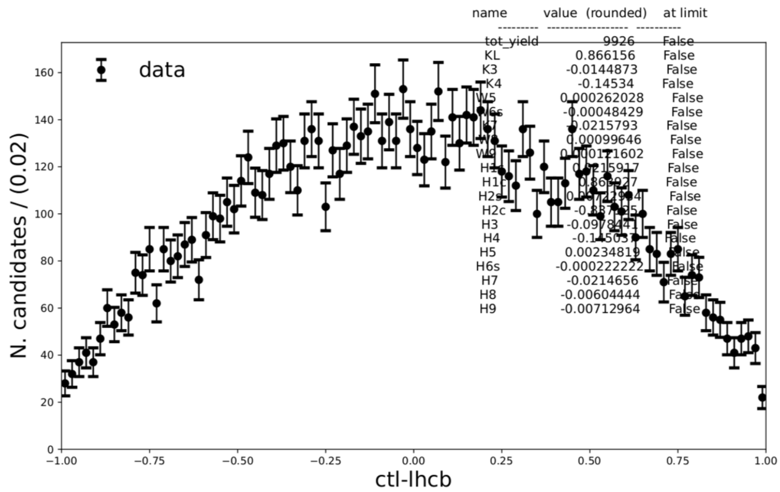

((b)) $\cos\theta_l$ - projection with mixing, i.e., $y \neq 0$..

Figure 20: Mixing vs. Non-Mixing projections of $\cos\theta_l$

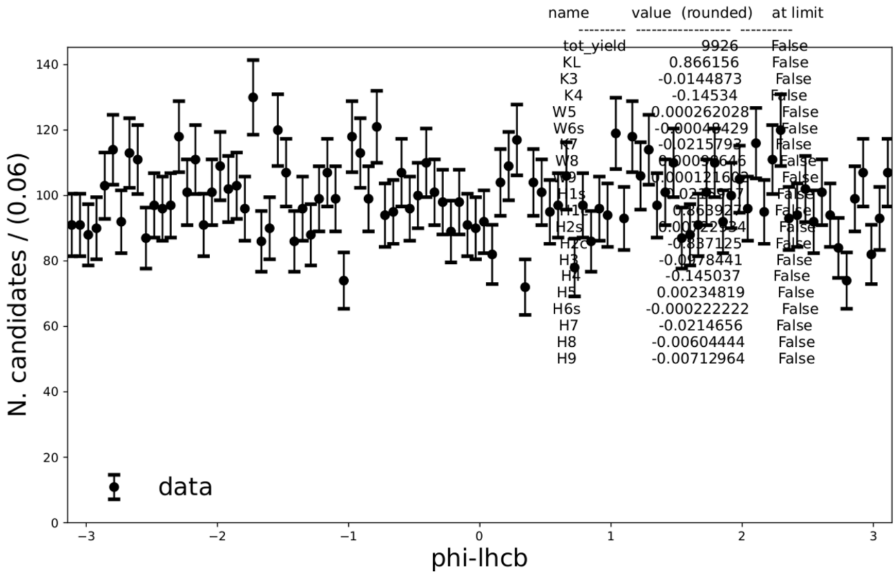

((a)) ϕ - projection no mixing, i.e., $y = 0$.

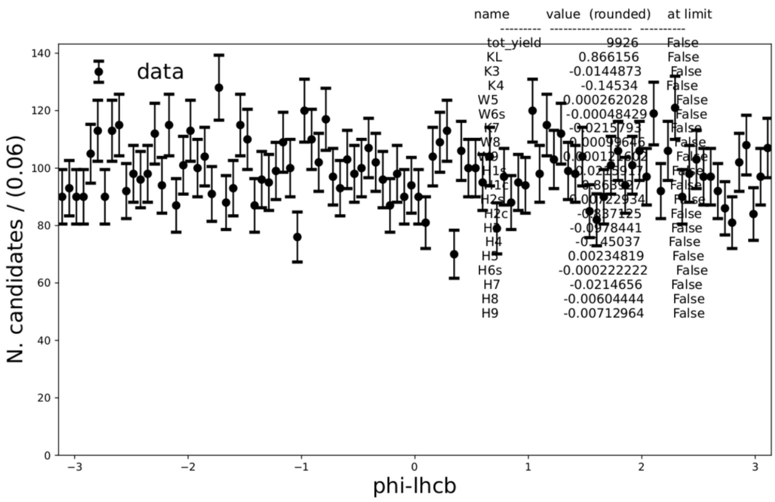

((b)) ϕ - projection with mixing, i.e., $y \neq 0$.

Figure 21: Mixing vs. Non-Mixing projections of ϕ

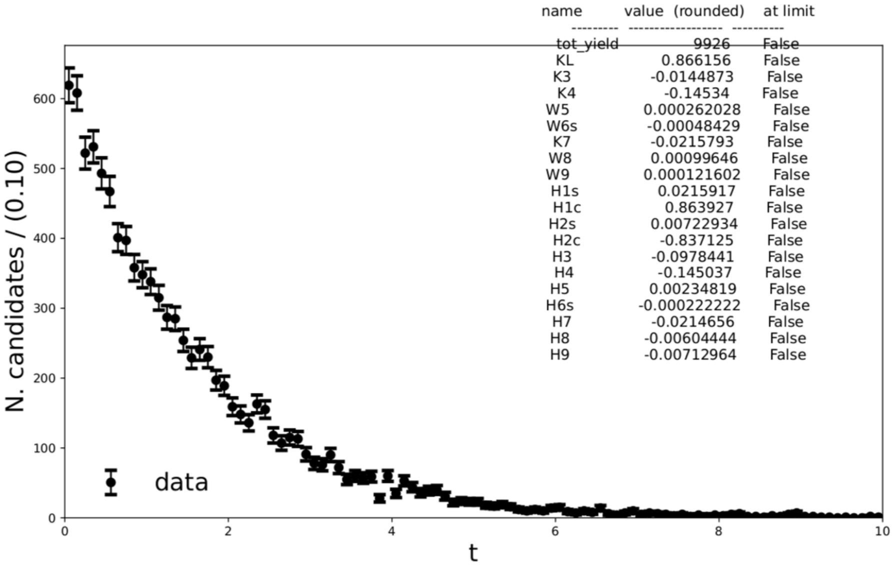

((a)) t - projection no mixing, i.e., $y = 0$.

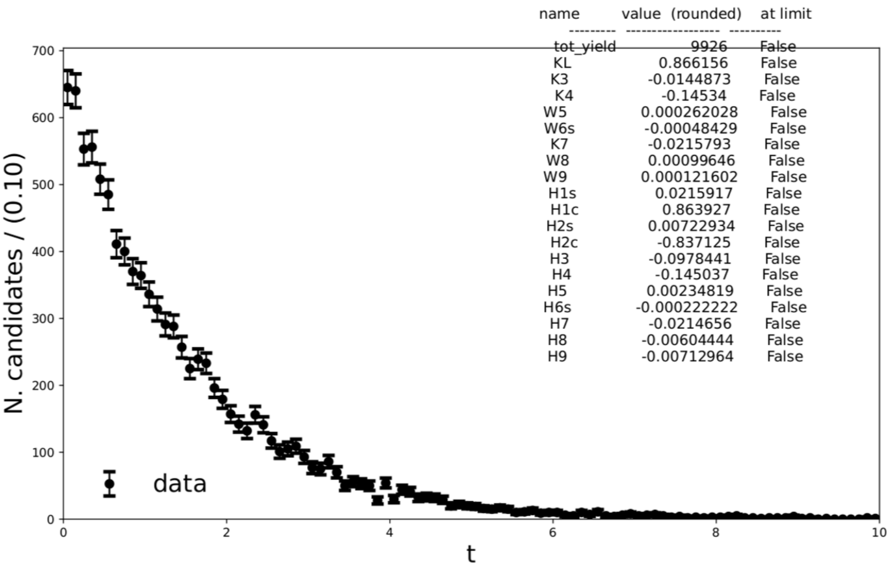

((b)) t - projection with mixing, i.e., $y \neq 0$.

Figure 22: Mixing vs. Non-Mixing projections of t

References

[1] R. Aaij, B. Adeva, M. Adinolfi, A. Affolder, Z. Ajaltouni, and et al. Akar. Observation of resonances consistent with pentaquark states in decays. *Physical Review Letters*, 115(7), August 2015.

[2] Henso Abreu, John Anders, Claire Antel, Akitaka Ariga, and Ariga et al. First direct observation of collider neutrinos with faser at the lhc. *Physical Review Letters*, 131(3),

July 2023.

[3] Wolfgang Altmannshofer, Patricia Ball, Aoife Bharucha, Andrzej J Buras, David M Straub, and Michael Wick. Symmetries and asymmetries ofb→k*+decays in the standard model and beyond. *Journal of High Energy Physics*, 2009(01):019–019, January 2009.

[4] Nima Arkani–Hamed, Savas Dimopoulos, and Gia Dvali. The hierarchy problem and new dimensions at a millimeter. *Physics Letters B*, 429(3–4):263–272, June 1998.

[5] G. Arnison, A. Astbury, B. Aubert, C. Bacci, G. Bauer, A. Bézaguet, R. Böck, T.J.V. Bowcock, M. Calvetti, T. Carroll, P. Catz, P. Cennini, S. Centro, F. Ceradini, S. Cittolin, D. Cline, C. Cochet, J. Colas, M. Corden, D. Dallman, M. DeBeer, M. Della Negra, M. Demoulin, D. Denegri, A. Di Ciaccio, D. DiBitonto, L. Dobrzynski, J.D. Dowell, M. Edwards, K. Eggert, E. Eisenhandler, N. Ellis, P. Erhard, H. Faissner, G. Fontaine, R. Frey, R. Frühwirth, J. Garvey, S. Geer, C. Ghesquière, P. Ghez, K.L. Giboni, W.R. Gibson, Y. Giraud-Héraud, A. Givernaud, A. Gonidec, G. Grayer, P. Gutierrez, T. Hansl-Kozanecka, W.J. Haynes, L.O. Hertzberger, C. Hodges, D. Hoffmann, H. Hoffmann, D.J. Holthuizen, R.J. Homer, A. Honma, W. Jank, G. Jorat, P.I.P. Kalmus, V. Karimäki, R. Keeler, I. Kenyon, A. Kernan, R. Kinnunen, H. Kowalski, W. Kozanecki, D. Kryn, F. Lacava, J.-P. Laugier, J.-P. Lees, H. Lehmann, K. Leuchs, A. Lévêque, E. Linglin, E. Locci, M. Loret, J.-J. Malosse, T. Markiewicz, G. Maurin, T. McMahon, J.-P. Mendiburu, M.-N. Minard, M. Moricca, H. Muirhead, F. Muller, A.K. Nandi, L. Naumann, A. Norton, A. Orkin-Lecourtois, L. Paoluzi, G. Petrucci, G.Piano Mortari, M. Pimiä, A. Placci, E. Radermacher, J. Ransdell, H. Reithler, J.-P. Revol, J. Rich, M. Rijssenbeek, C. Roberts, J. Rohlf, P. Rossi, C. Rubbia, B. Sadoulet, G. Sajot, G. Salvi, J. Salvini, J. Sass, A. Saudraix, A. Savoy-Navarro, D. Schinzel, W. Scott, T.P. Shah, M. Spiro, J. Strauss, K. Sumorok, F. Szoncso, D. Smith, C. Tao, G. Thompson, J. Timmer, E. Tscheslog, J. Tuominiemi, S. Van der Meer, J.-P. Vialle, J. Vrana, V. Vuillemin, H.D. Wahl, P. Watkins, J. Wilson, Y.G. Xie, M. Yvert, and E. Zurfluh. Experimental observation of isolated large transverse energy electrons with associated missing energy at s=540 gev. *Physics Letters B*, 122(1):103–116, 1983.

[6] M. Banner et al. Observation of Single Isolated Electrons of High Transverse Momentum in Events with Missing Transverse Energy at the CERN anti-p p Collider. *Phys. Lett. B*, 122:476–485, 1983.

[7] W. Bernreuther. Cp violation and baryogenesis, 2002.

[8] Christoph Bobeth, Gudrun Hiller, and Giorgi Piranishvili. Cp asymmetries in b → k*(→ k)lland untagged bs,bs→ (→k+k)lldecays at nlo. *Journal of High Energy Physics*, 2008(07):106–106, July 2008.

[9] Luisa Bonolis. Bruno Pontecorvo: From slow neutrons to oscillating neutrinos. *American Journal of Physics*, 73(6):487–499, 06 2005.

[10] V. M. Braun. Light-cone sum rules, 1998.

[11] Andrzej J. Buras. *Gauge Theory of Weak Decays: The Standard Model and the Expedition to New Physics Summits.* Cambridge University Press, 2020.

[12] Nicola Cabibbo. Unitary symmetry and leptonic decays. *Phys. Rev. Lett.*, 10:531–533, Jun 1963.

[13] Ashton B. Carter and A. I. Sanda. CP violation in b-meson decays. *Phys. Rev. D*, 23:1567–1579, Apr 1981.

[14] S.-K. Choi, S. L. Olsen, K. Abe, T. Abe, I. Adachi, and et al. Ahn. Observation of a narrow charmoniumlike state in exclusive decays. *Physical Review Letters*, 91(26), December 2003.

[15] V. De Sabbata and M. Gasperini. Neutrino Oscillations in the Presence of Torsion. *Nuovo Cim. A*, 65:479–500, 1981.

[16] L. Demortier and L. Lyons. Everything you always wanted to know about pulls.

[17] Sébastien Descotes-Genon, Joaquim Matias, and Javier Virto. Analysis of $B_{d,s}$ mixing angles in the presence of new physics and an update of $B_s \to \overline{k}^{0*} K^{0*}$. *Phys. Rev. D*, 85:034010, Feb 2012.

[18] Sébastien Descotes-Genon, Martín Novoa-Brunet, and K. Keri Vos. The time-dependent angular analysis of $B_d \to K_S \ell\ell$, a new benchmark for new physics. *JHEP*, 02:129, 2021.

[19] Sébastien Descotes-Genon and Javier Virto. Time dependence in $B \to V\ell\ell$ decays. *JHEP*, 04:045, 2015. [Erratum: JHEP 07, 049 (2015)].

[20] John Ellis. Higgs Physics. pages 117–168, 2015. 52 pages, 45 figures, Lectures presented at the ESHEP 2013 School of High-Energy Physics, to appear as part of the proceedings in a CERN Yellow Report.

[21] John Ellis, Mary K Gaillard, and Graham G Ross. Search for gluons in e+ e- annihilation. *Nuclear Physics B*, 111(2):253–271, 1976.

[22] F. Englert and R. Brout. Broken symmetry and the mass of gauge vector mesons. *Phys. Rev. Lett.*, 13:321–323, Aug 1964.

[23] Amand Faessler, Th. Gutsche, M. A. Ivanov, J. G. Körner, and V. E. Lyubovitskij. The exclusive rare decays $b \to k\bar{l}l$ and $b_c \to d(d^*)\bar{l}l$ in a relativistic quark model. *EPJ direct*, 4(1):1–33, December 2002.

[24] Davide Fazzini. Development of "same side" flavour tagging algorithms for measurements of flavour oscillations and CP violation in the B^0 mesons system, 2015. Presented 24 Mar 2015.

[25] Davide Fazzini. Flavour Tagging in the LHCb experiment. *PoS*, LHCP2018:230, 2018.

[26] Fermilab. Fermilab today archive - june 24, 2010. https://www.fnal.gov/pub/today/archive/archive_2010/today10-06-24.pdf, June 2010. Accessed: 2024-08-14.

[27] R. P. Feynman and M. Gell-Mann. Theory of the fermi interaction. *Phys. Rev.*, 109:193–198, Jan 1958.

[28] Murray Gell-Mann. Quarks. In *Elementary Particle Physics: Multiparticle Aspects*, pages 733–761. Springer, 1972.

[29] Diptimoy Ghosh, Marco Nardecchia, and S. A. Renner. Hint of lepton flavour non-universality in b meson decays. *Journal of High Energy Physics*, 2014(12), December 2014.

[30] Sheldon L Glashow. Partial-symmetries of weak interactions. *Nuclear physics*, 22(4):579–588, 1961.

[31] Jeffrey Goldstone, Abdus Salam, and Steven Weinberg. Broken symmetries. *Phys. Rev.*, 127:965–970, Aug 1962.

[32] Particle Data Group, P A Zyla, and et al. Barnett. Review of Particle Physics. *Progress of Theoretical and Experimental Physics*, 2020(8):083C01, 08 2020.

[33] Rajan Gupta. Introduction to lattice qcd, 1998.

[34] P.W. Higgs. Broken symmetries, massless particles and gauge fields. *Physics Letters*, 12(2):132–133, 1964.

[35] Kelly Izlar. The march of the penguin diagrams. https://www.symmetrymagazine.org/article/june-2013/the-march-of-the-penguin-diagrams?language_content_entity=und, June 2013. Accessed: 2024-08-14.

[36] David Kirkby and Yosef Nir. Cp violation in meson decays. *Review for the Particle Data Group*, 2006. URL: https://pdg.lbl.gov.

[37] Makoto Kobayashi and Toshihide Maskawa. CP-Violation in the Renormalizable Theory of Weak Interaction. *Progress of Theoretical Physics*, 49(2):652–657, 02 1973.

[38] Michal Kreps. Exotic meson studies at LHCb. *EPJ Web Conf.*, 81:04006, 2014.

[39] Frank Krüger, Lalit M. Sehgal, Nita Sinha, and Rahul Sinha. Angular distribution and cp asymmetries in the decays $\overline{B} \to K^-\pi^+e^-e^+$ and $\overline{B} \to \pi^-\pi^+e^-e^+$. *Phys. Rev. D*, 61:114028, May 2000.

[40] Jessica Levêque. Penguin domination. https://atlas.cern/updates/blog/penguin-domination, March 2014. Accessed: 2024-08-14.

[41] Marcel Materok. Angular analysis $B_s^0 \to \phi\mu^+\mu^-$ decays with the LHCb Experiment, 2023. Presented 05 Dec 2022.

[42] Joaquim Matias and Nicola Serra. Symmetry relations between angular observables in $\mathrm{B}^0 \to \mathrm{K}^*\mu^+\mu^-$ and the lhcb p_5' anomaly. *Physical Review D*, 90(3), aug 2014.

[43] MATTHIAS NEUBERT. Effective field theory and heavy quark physics. In *Physics In D ≥ 4 Tasi 2004*. WORLD SCIENTIFIC, July 2006.

[44] Nobel Prize Outreach AB. The nobel prize in physics 1979. NobelPrize.org, 2024. Accessed: Wed. 14 Aug 2024.

[45] Michael E. Peskin. *Concepts of Elementary Particle Physics.* Oxford University Press, 08 2019.

[46] Michael E. Peskin and Daniel V. Schroeder. *An Introduction to quantum field theory.* Addison-Wesley, Reading, USA, 1995.

[47] H. Poincaré. *Science and Method.* Cosimo, Incorporated, 2010.

[48] Matthew D. Schwartz. *Quantum Field Theory and the Standard Model.* Cambridge University Press, 2013.

[49] Mikhail Shifman. Itep lectures in particle physics, 1995.

[50] Mark Thomson. *Modern Particle Physics.* Cambridge University Press, 2013.

[51] David Tong. Lectures on quantum field theory. *Part III Cambridge University Mathematics Tripos, Michaelmas*, 2006.

[52] USLHC. Why do we expect a Higgs boson? Part II: Unitarization of Vector Boson Scattering, 2 2012.

[53] Wikipedia contributors. File: Standard Model of Elementary Particles.svg, 2023. [Online; accessed 15-August-2024].

[54] K. G. Wilson and W. Zimmermann. Operator product expansions and composite field operators in the general framework of quantum field theory. *Commun. Math. Phys.*, 24:87–106, 1972.

[55] Lincoln Wolfenstein. Parametrization of the kobayashi-maskawa matrix. *Phys. Rev. Lett.*, 51:1945–1947, Nov 1983.

[56] Dan-di Wu. A brief introduction to the strong cp problem.

[57] C. N. Yang and R. L. Mills. Conservation of isotopic spin and isotopic gauge invariance. *Phys. Rev.*, 96:191–195, Oct 1954.